Osteoblastic Lrp4 promotes osteoclastogenesis by regulating ATP release and adenosine-A_{2A}R signaling

Lei Xiong,[1,2,3] Ji-Ung Jung,[1,2] Hao-Han Guo,[1,2,3] Jin-Xiu Pan,[1,2,3] Xiang-Dong Sun,[1,2,3] Lin Mei,[1,2,3] and Wen-Cheng Xiong[1,2,3]

[1]Department of Neuroscience and Regenerative Medicine and [2]Department of Neurology, Medical College of Georgia, Augusta, GA 30912
[3]Charlie Norwood VA Medical Center, Augusta, GA 30912

Bone homeostasis depends on the functional balance of osteoblasts (OBs) and osteoclasts (OCs). Lrp4 is a transmembrane protein that is mutated in patients with high bone mass. Loss of Lrp4 in OB-lineage cells increases bone mass by elevating bone formation by OBs and reducing bone resorption by OCs. However, it is unclear how Lrp4 deficiency in OBs impairs osteoclastogenesis. Here, we provide evidence that loss of Lrp4 in the OB lineage stabilizes the prorenin receptor (PRR) and increases PRR/V-ATPase–driven ATP release, thereby enhancing the production of the ATP derivative adenosine. Both pharmacological and genetic inhibition of adenosine-$_{2A}$ receptor ($A_{2A}R$) in culture and Lrp4 mutant mice diminishes the osteoclastogenic deficit and reduces trabecular bone mass. Furthermore, elevated adenosine-$A_{2A}R$ signaling reduces receptor activator of nuclear factor κB (RANK)–mediated osteoclastogenesis. Collectively, these results identify a mechanism by which osteoblastic Lrp4 controls osteoclastogenesis, reveal a cross talk between $A_{2A}R$ and RANK signaling in osteoclastogenesis, and uncover an unrecognized pathophysiological mechanism of high-bone-mass disorders.

Introduction

Bone homeostasis depends on the functional balance of osteoblasts (OBs) and osteoclasts (OCs). Each releases secretable factors that regulate the function of the other. For example, OB-released factors include receptor activator of nuclear factor κB ligand (RANKL), osteoprotegerin (OPG), cytokine interleukin-33, and EphB4 (Yasuda et al., 1998; Teitelbaum, 2000; Zhao et al., 2006; Zaiss et al., 2011), among which RANKL is the best studied and perhaps most important (Yasuda et al., 1998; Teitelbaum, 2000). RANKL is necessary for trabecular bone structures, because RANKL deletion in osteocytes reduces OC number on cancellous bone and increases bone volume (BV; Nakashima et al., 2011; Xiong et al., 2011). Via its receptor, receptor activator of nuclear factor κB (RANK), RANKL increases nuclear factor κB signaling and promotes the commitment of bone marrow macrophages/monocytes (BMMs) to OC progenitors, OC differentiation, and activation (Yasuda et al., 1998; Teitelbaum, 2000). In contrast, OPG acts as an antagonist of RANKL to inhibit OC genesis and function (Teitelbaum, 2000). The ratio of RANKL to OPG is thus a key factor in the control of OC genesis. This ratio is up-regulated by multiple factors, including sclerostin Lrp4 (low-density lipoprotein [LDL] receptor–related protein 4) pathway (Itoh et al., 2000; Ma et al., 2001; Huang et al., 2004; Silvestrini et al., 2008; Wijenayaka et al., 2011; Xiong et al., 2015) and down-regulated by factors such as the canonical Wnt–β-catenin signaling pathway (Huang et al., 2004; Fujita and Janz, 2007; Silvestrini et al., 2008; Takahashi et al., 2011; Folestad et al., 2015).

Lrp4 is a member of LDL family receptors containing a large extracellular region with multiple LDLa, EGF-like, and β-propeller repeats; a transmembrane domain; and a short C-terminal region (Nakayama et al., 1998; Tian et al., 1999; Herz and Bock, 2002; Suzuki, 2004; Wu et al., 2010; Shen et al., 2015). It is a receptor for agrin to mediate neuromuscular junction formation and stability (Kim et al., 2008; Zhang et al., 2008; Wu et al., 2012; Zong et al., 2012; Shen et al., 2014). It is also a receptor for sclerostin to negatively regulate bone homeostasis (Li et al., 2005; Semënov et al., 2005; Choi et al., 2009; Leupin et al., 2011; Xiong et al., 2015). Mutations in Lrp4 and sclerostin genes have been identified in patients with high bone mass, such as sclerosteosis and Van Buchem disease (Balemans et al., 2002; Loots et al., 2005; Semënov et al., 2005; Leupin et al., 2011). Deletion of Lrp4 or sclerostin gene in mice results in high-bone-

Correspondence to Lin Mei: lmei@augusta.edu; or Wen-Cheng Xiong: wxiong@augusta.edu

Abbreviations used: $A_{2A}R$, adenosine-$_{2A}$ receptor; ANOVA, analysis of variance; BMM, bone marrow macrophage/monocyte; BMSC, bone marrow stromal cell; BV, bone volume; CM, conditioned medium; FCCP, carbonyl cyanide-p-trifluoromethoxyphenylhydrazone; LDL, low-density lipoprotein; M-CSF, macrophage colony-stimulating factor; μCT, micro–computed tomography; MNC, multinuclei cell; OB, osteoblast; OC, osteoclast; Ocn, osteocalcin; OCR, oxygen consumption rate; OPG, osteoprotegerin; PEI, polyethylenimine; PPi, pyrophosphate; PRR, prorenin receptor; P/S, penicillin/streptomycin; PYD, pyridinoline; RANK, receptor activator of nuclear factor κB; RANKL, RANK ligand; TRAP, tartrate-resistant acid phosphatase; TV, total volume; WT, wild type.

The Rockefeller University Press $30.00
J. Cell Biol. Vol. 216 No. 3 761–778
https://doi.org/10.1083/jcb.201608002

mass deficits (Chang et al., 2014; Ryan et al., 2015; Xiong et al., 2015). Lrp4 deficiency in OB-lineage cells promotes bone formation by attenuating sclerostin inhibition of Wnt–β-catenin signaling and OB differentiation (Chang et al., 2014; Xiong et al., 2015). Interestingly, Lrp4-deficiency in OB-lineage cells also impairs OC-mediated bone resorption (Xiong et al., 2015). However, the underlying mechanisms remain unclear.

Here, we show that osteoblastic Lrp4 suppresses prorenin receptor (PRR)/V-ATPase–dependent vesicular ATP release, thus decreasing extracellular ATP derivatives, pyrophosphate (PPi), and adenosine. Inactivation of adenosine–adenosine-$_{2A}$ receptor ($A_{2A}R$) signaling in Lrp4 mutant mice diminished the OC genesis deficit and reduced trabecular bone mass. Activation of $A_{2A}R$ signaling in BMMs decreased RANK levels. These results reveal unrecognized function of osteoblastic Lrp4 to negatively regulate PRR/V-ATPase activity, demonstrate important roles for osteoblastic ATP release and adenosine-$A_{2A}R$ signaling in suppression of RANKL-driven osteoclastogenesis, and reveal a novel mechanistic insight into intricate interaction between OBs and OCs in bone homeostasis.

Results

Reduced OC differentiation of BMMs from osteoblastic Lrp4 mutant mice

To explore mechanisms of how osteoblastic Lrp4 knockout results in an OC genesis deficit, we first tested whether this deficit could be rescued by treatment with RANKL, a crucial factor necessary for OC genesis that is reduced in Lrp4-deficient OB-lineage cells (Xiong et al., 2015). BMMs were treated with exogenous RANKL to induce OC differentiation (Fig. 1 A). BMMs from control mice formed OC-like, tartrate-resistant acid phosphatase (TRAP)$^+$ multinuclei cells (MNCs) at day 7 of treatment (Fig. 1 B). However, the number of TRAP$^+$ MNCs was much lower in BMMs from mr-Lrp4^{mitt} (muscle-rescued Lrp4-null mutant) mice, even after treatment with 100 ng/ml RANKL, a concentration four times the sufficient dose of 25 ng/ml, for 7 d (Fig. 1, B and C), suggesting an OC differentiation deficit. Such a deficit was also observed in BMMs from OB-selective conditional knockout (Lrp4^{Ocn}-cko) mice (or Lrp-4$^{f/f}$; osteocalcin [Ocn]–Cre; Fig. 1, D–G). The OC differentiation deficit was detected in BMMs from 3-mo-old mice (Fig. 1, F and G), but not 1-mo-old mice (Fig. 1, D and E), in agreement with the time of Ocn promoter activation and thus Lrp4 conditional knockout (Zhang et al., 2002; Xiong et al., 2015). In addition, this deficit was detected on day 7, but not day 14, of RAN KL treatments during the OC differentiation assay (Fig. 1, F and G). These results indicate a transient RANKL-induced OC differentiation deficit in BMMs from OB-Lrp4 mutant mice, suggesting an unexpected mechanism.

Next, we performed FACS analyses to determine whether the number of OC progenitor cells in BMMs from OB-Lrp4 mutant mice was reduced. BMMs isolated from 3-mo-old mice were sorted with antibodies against CD11b (a macrophage/monocyte marker) and RANK (a receptor for RANKL expressed in OC progenitor cells; Fig. 1 A). Approximately 99% of BMMs of all genotypes were positive for CD11b (CD11b$^+$; Fig. 1, H and I), indicating that they belong to macrophage/monocyte cells. However, the percentage of RANK$^+$ cells was significantly lower in BMMs from OB-Lrp4 mutant mice than in those of control mice (Fig. 1, H and J), suggesting a problem with OC progenitor cell production. In accord, the RANK protein level was markedly lower in BMMs from Lrp4 mutant mice than in control mice (Fig. 1, K and L). The level of c-Fms, a receptor for macrophage colony-stimulating factor (M-CSF), was similar between control and mutant BMMs, indicating normal development of macrophages. These results suggest that OB-Lrp4 may promote the commitment of BMMs to RANK$^+$ OC precursor cells in the bone marrow.

We then determined whether the conditioned medium (CM) of Lrp4-deficient OB-lineage cells contains an inhibitor of OC differentiation. We collected CMs from wild-type (WT) and OB-Lrp4 mutant bone marrow stromal cells (BMSCs); WT BMMs were treated with the different CMs for 7 d in the presence of M-CSF and RANKL and subjected to TRAP staining for OC formation (Fig. 1 M). As shown in Fig. 1 (N–O), the number of TRAP$^+$ MNCs was lower in BMMs treated with Lrp4^{mitt}-BMSC CM that in those treated with WT-BMSC CM. These results indicate that OB-Lrp4 mutant BMSCs regulate OC genesis via secretable factors (Fig. 1 P).

Increased ATP, PPi, and adenosine in extracellular compartments of Lrp4-deficient OB-lineage cells

To identify the secretable factors that inhibit OC genesis, we first examined levels of SOST and Wise in CMs of WT and Lrp4-deficient BMSCs, because both SOST and Wise are believed to be Lrp4 ligands important for bone homeostasis and their serum levels are increased in Lrp4 mutant mice (Ahn et al., 2013; Chang et al., 2014; Xiong et al., 2015; Fijalkowski et al., 2016). As shown in Fig. 2 (A and B), the levels of both SOST and Wise were comparable in CMs of two genotypes of BMSCs, eliminating the possibility that SOST and Wise are involved in OC differentiation inhibition.

We next measured PPi, because it is known to inhibit OC differentiation (Nishikawa et al., 1996; Baron et al., 2011; Burr and Russell, 2011; Russell, 2011). Intriguingly, levels of PPi were much higher in CMs of Lrp4 mutant BMSCs and OBs than in those of controls (Fig. 2 C). PPi is derived from ATP metabolism (Russell, 2011), and both ATP and ATP's hydrolytic product adenosine are implicated in the regulation of OC genesis (Mediero and Cronstein, 2013; Idzko et al., 2014). We thus determined whether ATP and adenosine in CMs were altered by Lrp4 deficiency. As shown in Fig. 2 (D and E), levels of both were also elevated in CMs of Lrp4-deficient BMSCs and OBs compared with those of controls. Further characterization indicates that Lrp4-deficiency–mediated ATP increase in the extracellular compartment was time dependent, detectable at day 1, and peaked at day 3 in cultures of Lrp4-deficient OB-lineage cells (Fig. S1 A). The mRNAs of CD39 and CD73, which produce enzymes of PPi and adenosine from ATP, respectively (Prosdocimo et al., 2009; Sauer et al., 2012; Mahamed et al., 2015), were unchanged in Lrp4-deficient OB-lineage cells (Fig. S1, B and C), suggesting that high levels of PPi and adenosine are caused by higher levels of ATP.

To understand how Lrp4 deficiency in OB-lineage cells results in higher levels of ATP in their extracellular compartments, we measured total intracellular ATP levels and examined mitochondrial respiratory capacity, an event critical for intracellular ATP synthesis. The total intracellular ATP levels in Lrp4 mutant BMSCs and OBs were unchanged compared with those of controls (Fig. 2 F). However, using the Seahorse

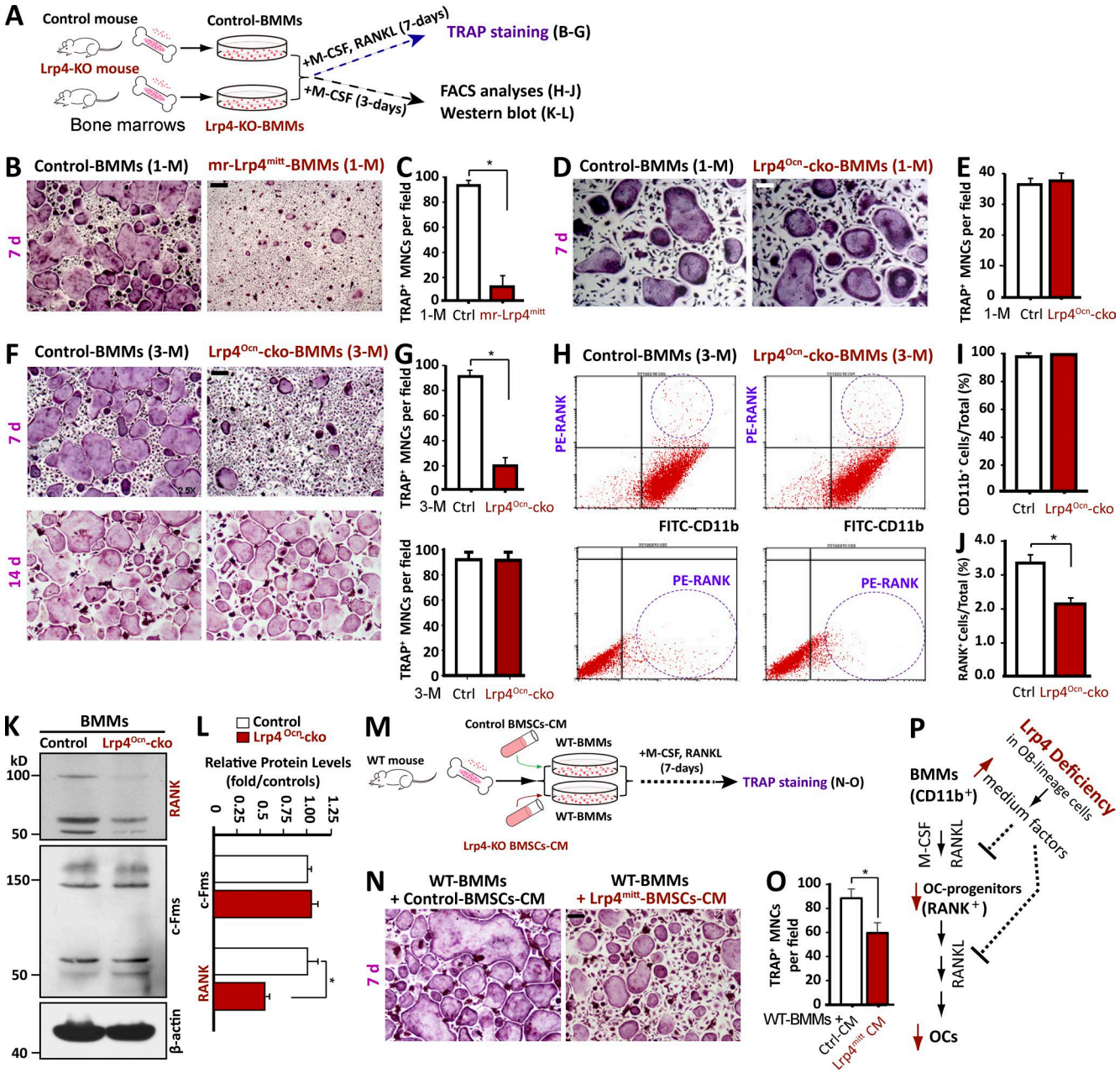

Figure 1. **Reduced OC differentiation in BMMs from osteoblastic Lrp4 mutant mice or BMMs treated with CM of Lrp4-deficient OB-lineage cells.** (A–G) TRAP staining analysis of cultured OCs derived from BMMs of different genotypes. (A) Experimental strategy. Cells were treated with 100 ng/ml RAN KL for 7 or 14 d as indicated. Representative images are shown in B, D, and F, and quantitative data of TRAP+ multinuclei cells (MNCs; more than three nuclei) per randomly selected visual field are shown in C, E, and G. Bars, 100 µm. Data represent mean ± SD from three different cultures; *, P < 0.05. (H) FACS analysis of primary BMMs. Bone marrow was isolated from the indicated mice and incubated overnight. BMMs were isolated from nonadherent cells by Ficoll-Hypaque gradient centrifugation and analyzed by FACS with antibodies against CD11b and RANK. (I and J) Quantitative data of FACS analysis. Data represent mean ± SD, *n* = 3; *, P < 0.05. (K and L) Western blot analysis of RANK and c-Fms expression in BMMs from indicated mice. Data represent mean ± SD, *n* = 3; *, P < 0.05. (M–O) TRAP staining of WT BMMs in the presence of CM of WT or Lrp4mitt BMSCs. (M) Experimental strategy. (N) Representative images. Bar, 100 µm. (O) Quantitative data of TRAP+ MNCs in N. Data represent mean ± SD, *n* = 3; *, P < 0.05. (P) Illustration of a working model. Lrp4-deficient OB-lineage cells release secretable factors to reduce OC differentiation.

platform to measure oxygen consumption rates (OCRs) and mitochondrial respiratory capacity in real time, we detected higher rates of both basal oxygen consumption and maximal respiratory capacity, which were induced by the mitochondrial uncoupler FCCP (carbonyl cyanide-p-trifluoromethoxyphenyl-hydrazone) in Lrp4-deficient OBs than in those of controls (Fig. 2, G and H). No difference in oxygen consumption was observed after treatment of cells with oligomycin, an inhibitor of ATP synthase (Fig. 2, G and H). These results thus indicate hyperfunctional mitochondria in Lrp4-deficient OBs, in line with the previous studies of hyper-OB function in Lrp4 mutant mice (Chang et al., 2014; Xiong et al., 2015).

Collectively, these observations support the notion that Lrp4 deficiency in OB-lineage cells increases both ATP synthesis and secretion, which then increases levels of PPi and adenosine (Fig. 2 I).

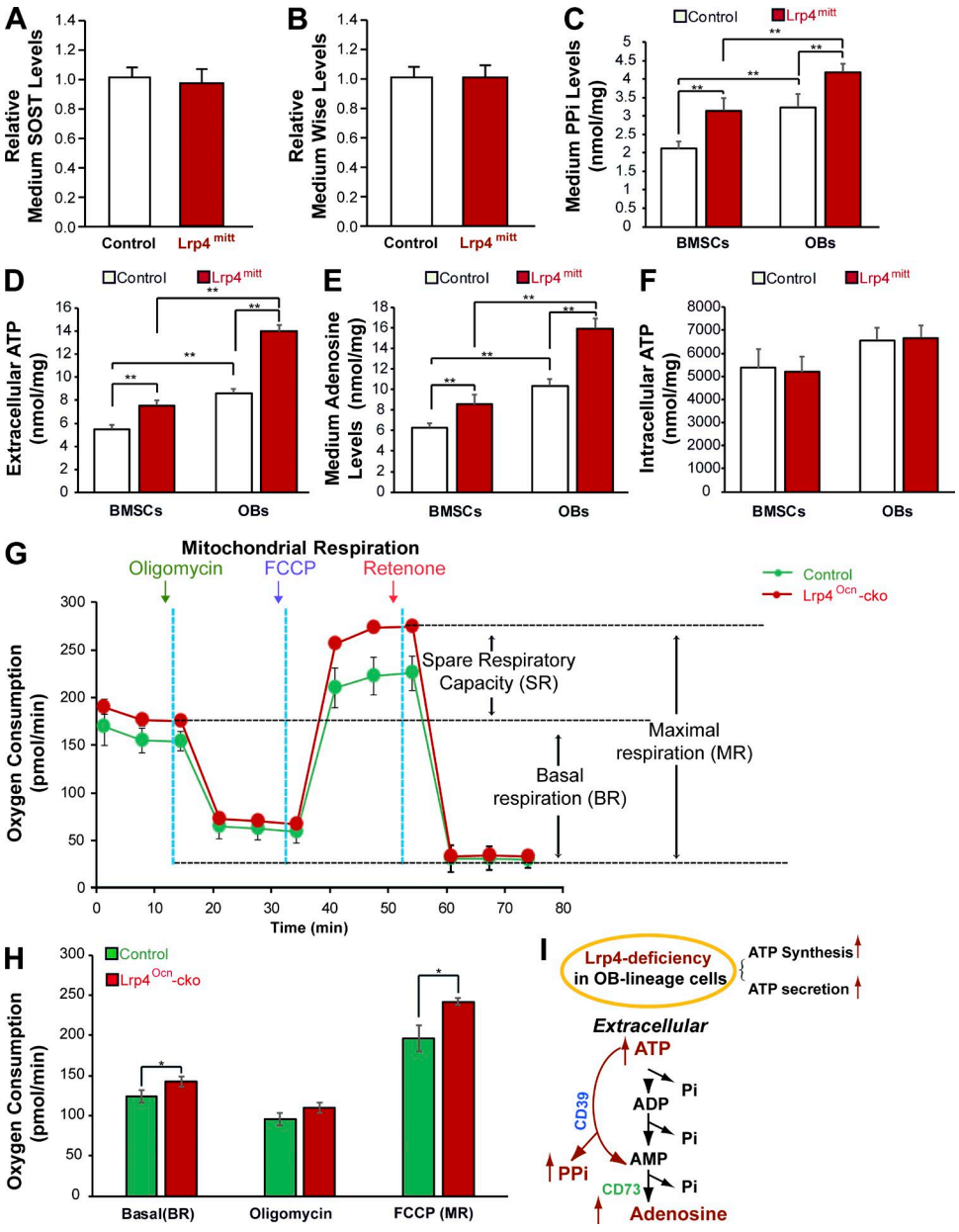

Figure 2. **Increased levels of ATP, PPi, and adenosine in CMs of Lrp4-deficient OB-lineage cells.** CMs of Lrp4-deficient BMSCs or OBs were subjected to the indicated analyses as detailed in Materials and methods. (A and B) No changes in SOST or Wise levels were detected. Data represent mean ± SD, *n* = 3. (C–E) Increased ATP, PPi, and adenosine levels were detected. PPi, ATP, and adenosine levels were measured in the same amounts of culture medium that were collected from the same number of control and mutant cells plated on culture dishes for 3 d. The protein concentrations (in milligrams) of cell lysates were also determined and used to normalize the concentrations (in nanomoles per milliliter) of PPi, ATP, and adenosine. Data represent mean ± SD, *n* = 3; **, P < 0.001. (F) Intracellular ATP levels in lysates of Lrp4-deficient BMSCs or OBs. Data represent mean ± SD, *n* = 3; **, P < 0.001. (G and H) An increased oxygen consumption rate (OCR) was detected in Lrp4-deficient OBs by using a Seahorse XF96 analyzer. For validation of the measurements, we used the ATP synthase inhibitor 2 µM oligomycin after recording a basal line, followed by treatment with 3 µM of the pharmaceutical uncoupler FCCP and 1 µM of the complex I inhibitor rotenone. Representative traces of OCRs are indicated in G, and quantification data (mean ± SEM, *n* = 3; *, P < 0.05) are presented in H. (I) Illustration of a model where Lrp4 deficiency in OB-lineage cells increased ATP secretion, consequently elevating PPi and adenosine levels.

Inhibition of adenosine-A_{2A}R signaling diminishes the OC differentiation deficit

PPi is known to inhibit not only OC genesis but also bone mineralization (Nishikawa et al., 1996; Russell, 2011; Orriss et al., 2013). However, previous studies, including ours, have demonstrated an increased bone mineralization in Lrp4 mutant mice (Leupin et al., 2011; Chang et al., 2014; Xiong et al., 2015). Serum levels of PPi were comparable between Lrp4 mutant mice and control mice (Fig. S1 D). These results suggest that PPi may play little to no role in Lrp4-deficient mice, although it was increased in cultured Lrp4-deficient OB-lineage cells.

Activation of adenosine receptor A_{2A}R has been shown to inhibit OC genesis (Mediero and Cronstein, 2013). We thus determined whether adenosine-A_{2A}R signaling is involved in the OC genesis deficit by Lrp4 mutation. WT BMMs were treated with CMs of control and Lrp4 mutant BMSCs in the presence of SCH58261, an A_{2A}R antagonist (Fig. 3 A). As shown in Fig. 3

(B and C), in vitro OC genesis (TRAP+ MNC formation) was impaired when treated with CM of Lrp4-deficient BMSCs; this effect was diminished by SCH58261. In contrast, A740003, an antagonist of the P_2X_7 receptor (P_2X_7R), showed little effect on the formation of TRAP+ MNCs (Fig. 3, B and C). These results suggest that inhibition of adenosine-$A_{2A}R$ signaling could diminish the OC genesis deficit.

To test this hypothesis in vivo, Lrp4^{Ocn}-cko mice at age postnatal day 70 were treated with SCH58261 (i.p., 2 mg/kg, daily) for 5 wk (Fig. 4 A), and their long bone samples were subjected to micro–computed tomography (μCT) analysis 5 wk later. As shown in Fig. 4 (B and C), SCH58261 reduced trabecular bone mass in Lrp4^{Ocn}-cko mice compared with vehicle controls. This effect appeared to be selective, as SCH58261 did not affect cortical BV (Fig. 4, B and C) and had a lesser effect on control (Ocn-Cre) mice (Fig. 4, B and C). Although SCH58261 increased TRAP+ OCs and levels of serum pyridinoline (PYD) and calcium (markers of bone resorption; Fig. 4, D–G), it had no effect on serum Ocn levels (Fig. 4 H). In addition, although SCH58261 fully restored the number of TRAP+ cells in trabecular bone regions of Lrp4^{Ocn}-cko mice (Fig. 4, D and E), its rescue effect on bone resorption (measured by serum levels of PYD and calcium) appeared to be partial (Fig. 4, F and G). These results indicate that inhibiting $A_{2A}R$ improves OC formation and activation in Lrp4 mutant mice. As a control, treatment of Lrp4^{Ocn}-cko mice with A740003 (i.p., 2.75 mg/kg; Fig. S2, A–E) had no effect on bone resorption markers (TRAP+ OC and serum PYD; Fig. S2, F–H), in agreement with in vitro studies (Fig. 3, B and C). However, the treatment decreased trabecular bone mass (Fig. S2, B and C) and levels of serum Ocn (Fig. S2 I), a marker of bone formation. These results indicate that SCH58261 and A740003 have differential effects on OC-mediated bone resorption and OB-mediated bone formation in Lrp4 mutant mice and provide additional evidence for adenosine-$A_{2A}R$ signaling in OC formation and activation in Lrp4^{Ocn}-cko mice.

To further explore $A_{2A}R$'s function in the OC genesis deficit by Lrp4 mutation, we crossed Lrp4^{Ocn}-cko mice with $A_{2A}R$-null ($A_{2A}R$-KO) mice. The resulting Lrp4^{Ocn}-cko;$A_{2A}R$-KO mice were subjected to μCT analysis and used for an in vitro OC genesis assay. Indeed, μCT analysis showed a reduced trabecular bone mass in Lrp4^{Ocn}-cko;$A_{2A}R$-KO mice compared with Lrp4^{Ocn}-cko mice (Fig. 5, A and B), in agreement with the results of SCH58261 treatment. A marked reduction of trabecular bone mass was detected in $A_{2A}R$-KO mice compared with WT controls (Fig. 5, A and B), in line with previous studies (Mediero et al., 2012, 2013). TRAP+ cells and bone resorption (serum PYD) were elevated in Lrp4^{Ocn}-cko;$A_{2A}R$-KO mice compared with Lrp4^{Ocn}-cko mice (Fig. 5, C–F). In agreement, in vitro OC genesis assays showed that the number of TRAP+ MNCs was higher in Lrp4^{Ocn}-cko;$A_{2A}R$-KO BMMs than in Lrp4^{Ocn}-cko BMMs (Fig. 6, A and B). These results suggest a negative role of $A_{2A}R$ in OC differentiation in vitro and in vivo. Intriguingly, whereas $A_{2A}R$-KO had little effect on RAN KL/OPG expression in BMSCs (Fig. 6, C and D), Western blot and FACS analyses demonstrated that it restored RANK levels in BMMs from Lrp4^{Ocn}-cko mice (Fig. 6, E–H). These results suggest that $A_{2A}R$ may inhibit OC genesis by suppressing RANK signaling and/or the commitment of BMMs to RANK+ OC precursor cells in the bone marrow. This view was further supported by the finding that treatment of

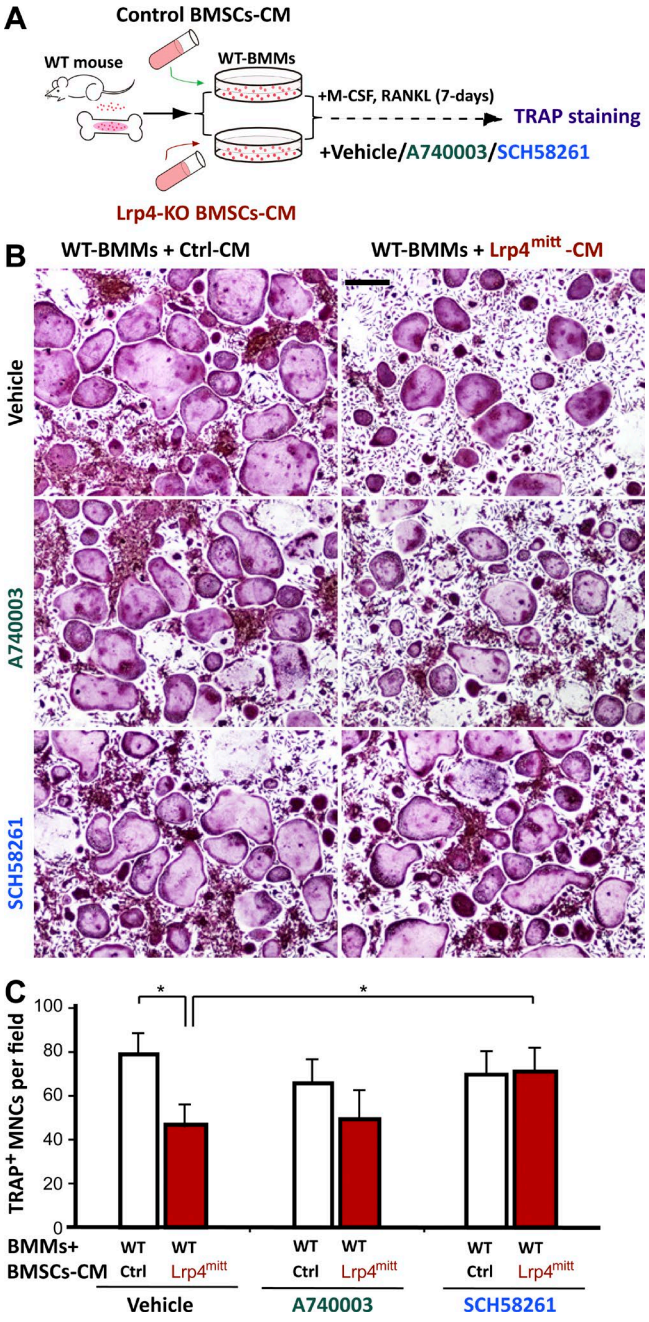

Figure 3. **Blocking $A_{2A}R$ using SCH58261 diminished the OC genesis deficits caused by Lrp4^{mitt} CM.** (A) Experimental strategy. TRAP staining of WT BMMs that were treated with CM of WT or Lrp4^{mitt} BMSCs. PBS control, 10 nM A740003, or 25 nM SCH58261 was added to the culture medium before BMM treatments. (B) Representative images of the cultures treated with CM plus RANKL for 7 d. Bar, 150 μm. (C) Quantitative analyses of TRAP+ multinuclei cells (MNCs) per field. Mean ± SD values from three different cultures are shown. *, $P < 0.05$.

WT BMMs with high concentrations of 150 μM adenosine decreased RANK levels, and this decrease was prevented by SCH58261 (Fig. 6, I and J).

In aggregate, these results suggest that the impairment in OC genesis (including commitment of BMMs to RANK+ OC precursor cells, OC formation, and activation) in Lrp4 mutant mice is likely caused by increased adenosine-$A_{2A}R$ signaling.

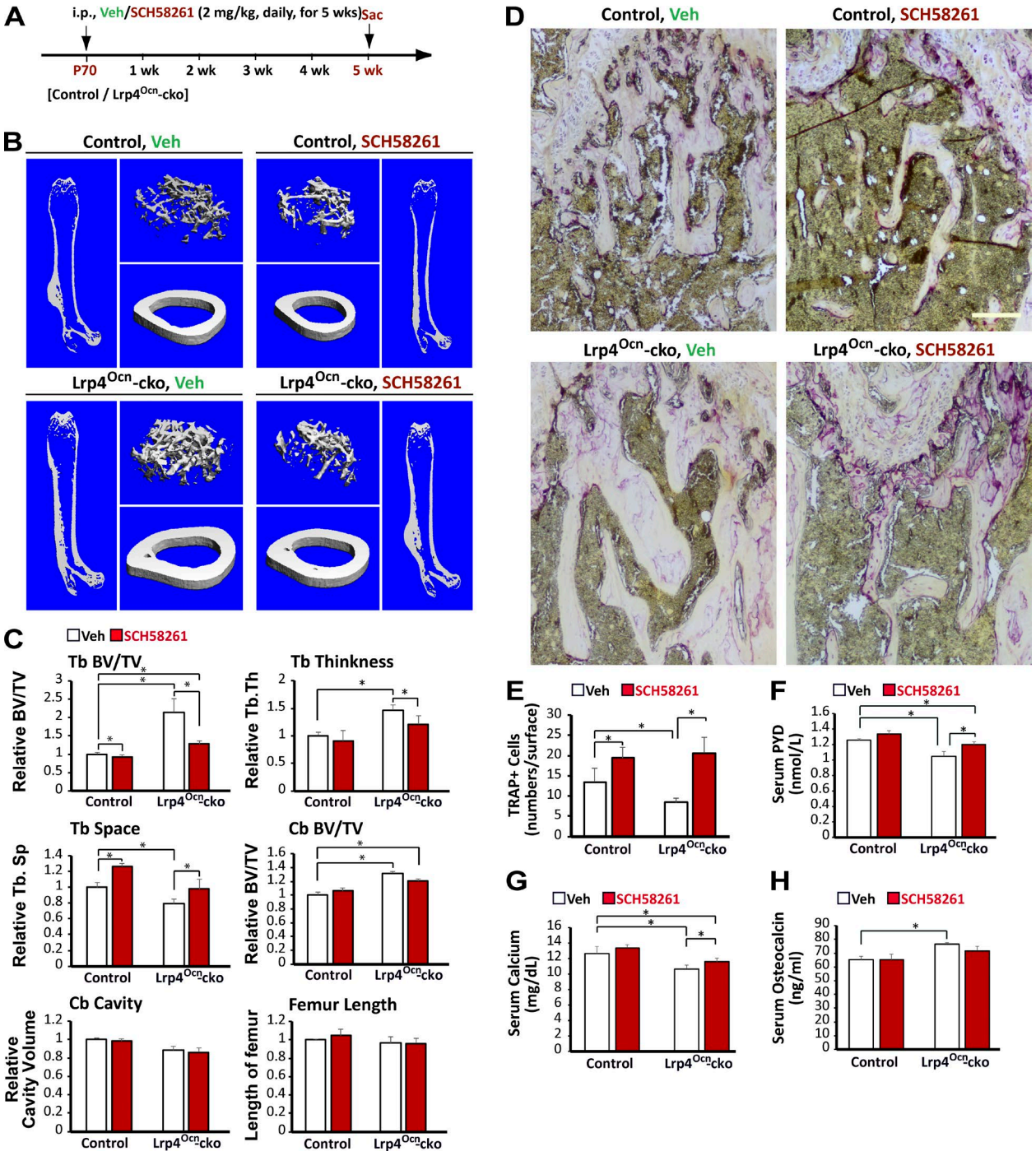

Figure 4. **Blocking $A_{2A}R$ by SCH58261 diminished high-bone-mass deficit in Lrp4^{Ocn}-cko mice.** (A) Experimental strategy. Postnatal day 70 (P70) control (Ocn-Cre) and Lrp4^{Ocn}-cko mice were administered a once-daily intraperitoneal injection of 2 mg/kg SCH48261 or vehicle (0.9% sodium chloride) for 5 wk. The femurs and sera samples collected after treatments were subjected to µCT and ELISA/RIA assays, respectively. (B and C) The µCT analysis of femurs from control and Lrp4^{Ocn}-cko littermates. Five different male mice of each genotype per group were examined blindly. Representative 3D images are shown in B. Quantification analyses (n = 5) of trabecular bone (TB) volumes over total volumes (BV/TV), TB thickness (TB. Th), TB space (Tb. Sp), cortical bone (CB) BV/TV, CB cavity, and femur length by direct model of µCT analysis are presented in C. Data were analyzed by two-way ANOVA; *, $P < 0.05$. (D and E) TRAP staining analysis of femur sections. Bar, 100 µm. Quantification analysis is shown in E as mean ± SD (n = 5 femur samples for each group). (F–H) RIA analysis of serum pyridinoline (PYD) and osteocalcin (Ocn) levels, and colorimetric analysis of serum calcium levels. Values are presented as mean ± SD (n = 5). *, $P < 0.05$.

Elevated V-ATPase–driven vesicular ATP loading and release in Lrp4-deficient OB-lineage cells

We next investigated the mechanisms by which osteoblastic Lrp4 regulates ATP release. First, we characterized the inhibitory effect of various chemicals on ATP release from Lrp4 mutant BMSCs. Because vesicular ATP release is thought to contribute to extracellular ATP levels in OBs (Orriss et al., 2009, 2013), we initially tested the effect of bafilomycin A1 (BafA1), an inhibitor of V-ATPase. At commonly used

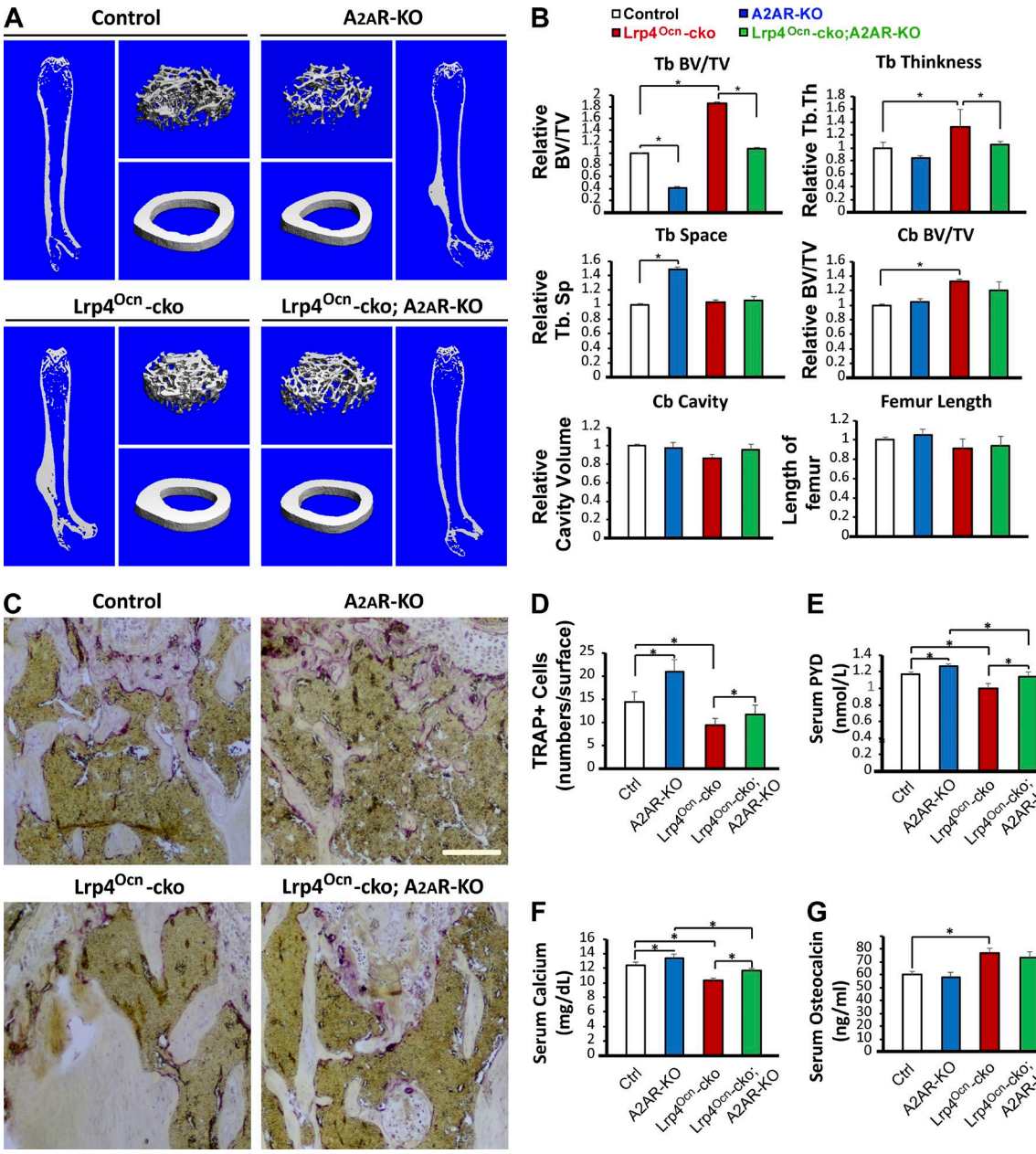

Figure 5. **Diminished high-bone-mass phenotype in Lrp4^{Ocn}-cko mice by A_{2A}R knockout.** The femurs and sera samples collected from 3-mo-old control (Ocn-Cre), A_{2A}R-KO, Lrp4^{Ocn}-cko, and Lrp4^{Ocn}-cko;A_{2A}R-KO mice were subjected to μCT and ELISA/RIA analyses. (A and B) μCT analysis. Five different male mice of each genotype per group were examined blindly. Representative 3D images are shown in A. Quantification analyses of trabecular bone (TB) volumes over total volumes (BV/TV), TB thickness (TB. Th), TB space (Tb. Sp), cortical bone (CB) BV/TV, CB cavity, and femur length by direct model of μCT analysis are presented in B. Data were analyzed by two-way ANOVA; *, $P < 0.05$. (C and D) TRAP staining analysis. Representative images are shown in C. Bar, 50 μm. Quantification analysis (mean ± SD, $n = 5$ femur samples for each group) are shown in D. (E–G) RIA analyses of serum PYD and Ocn, and colorimetric analysis of serum calcium levels. Values are presented as mean ± SD ($n = 5$). *, $P < 0.05$.

concentrations (e.g., 100 nM; Bowman et al., 1988; Zhang et al., 1994; Robinson et al., 2004), BafA1 inhibited ATP release from WT BMSCs, which may have complicated the interpretation of results from Lrp4 mutant BMSCs (Fig. 7 A). At 10 nM, however, BafA1 had no effect on ATP release from WT BMSCs (Fig. 7 A); in contrast, it abolished increased ATP release from Lrp4 mutant BMSCs (Fig. 7 A), suggesting an enhanced V-ATPase–dependent ATP release. The proton gradient is important for ATP loading into lysosomes (Coco et al., 2003; Tokunaga et al., 2010). To test the hypothesis further, Lrp4 mutant BMSCs were treated with chloroquine (a lysosomotropic agent that buffers pH in lysosomes; Chen et al., 2011). At a concentration of 5 μM, which had no effect on ATP release from WT BMSCs, chloroquine inhibited ATP release from Lrp4 mutant BMSCs (Fig. 7 B), further supporting the hypothesis. P_2X_7R has been implicated the release of ATP release in an autocrine manner (King, 2007; Takai et al., 2014). However, treatment of Lrp4 mutant BMSCs with A740003 had no effect on ATP release (Fig. 7 C). Similar results were also observed in Lrp4 mutant OBs (Fig. S3 A). These results suggest that Lrp4 deficiency in OB-lineage cells may increase V-ATPase–dependent ATP release.

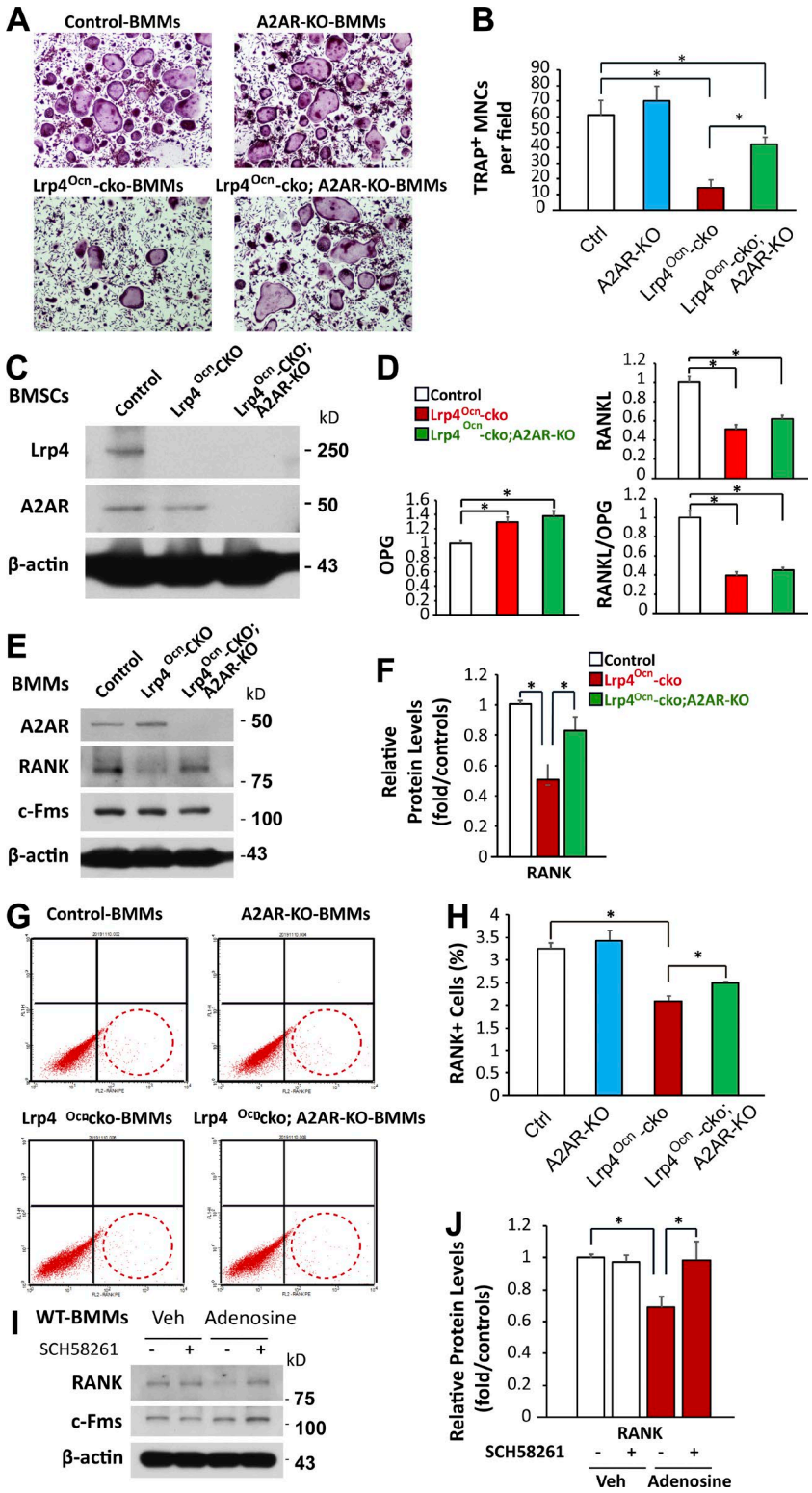

Figure 6. **Reduced OC genesis deficits in Lrp4^{Ocn}-cko mice by $A_{2A}R$ knockout.** (A and B) TRAP staining analysis. BMMs of 3-mo-old control (Ocn-cre), $A_{2A}R$-KO, Lrp4^{Ocn}-cko, and Lrp4^{Ocn}-cko;$A_{2A}R$-KO mice were cultured for 7 d in the presence of 100 ng/ml RANKL and M-CSF. Representative images are shown in A. Bar, 100 µm. Quantitative analyses of TRAP$^+$ multinuclei cells (MNCs) per field are presented in B. Shown are mean ± SD values from three different cultures. *, $P < 0.05$. (C) Western blot analysis of Lrp4 and $A_{2A}R$ expression in BMSCs derived from control (Ocn-cre), Lrp4^{Ocn}-cko, and Lrp4^{Ocn}-cko;$A_{2A}R$-KO mice. (D) Real-time PCR analysis of RANKL and OPG expression in BMSCs derived from the indicated mice. Data are shown as mean ± SD, $n = 3$; *, $P < 0.05$. (E and F) Western blot analysis of RANK and c-Fms expression in BMMs from indicated mice. Data are shown as mean ± SD, $n = 3$; *, $P < 0.05$. (G and H) FACS analysis of primary BMMs. Bone marrow isolated from the indicated mice was incubated overnight in the presence of M-CSF. BMMs isolated from nonadherent cells by Ficoll-Hypaque gradient centrifugation were analyzed by FACS with antibodies against RANK. Quantitative data (mean ± SD, $n = 3$; *, $P < 0.05$) are shown in H. (I and J) BMMs derived from 3-mo-old WT mice were treated with the indicated agents (150 µM adenosine, 25 nM SCH58261) in the presence of M-CSF for 6 d, and culture media were changed every day. Cell lysates were subjected to Western blot analyses with the indicated antibodies. Representative blots are shown in I, and quantitative results (mean ± SD, $n = 3$; *, $P < 0.05$) are presented in J.

Second, we measured the activity of V-ATPase in WT and Lrp4 mutant BMSCs using in vitro ATP hydrolysis assay. As shown in Fig. 7 D, V-ATPase was more active in Lrp4-deficient cells than in controls. Third, we measured the pH in lysosomes, because V-ATPase is a proton pump that is essential for the vesicular proton gradient and acidification (Bankston and Guidotti, 1996; Rudnick, 2008; Wang and Hiesinger, 2013), and the proton gradient controls vesicular ATP loading (Coco et al., 2003; Tokunaga et al., 2010). As shown in Fig. 7 (E and F), vesicular fluorescence of LysoSensor (a pH sensor) was higher in Lrp4-deficient BMSCs than in controls, indicating increased vesicular acidification and providing additional support for elevated V-ATPase activity in Lrp4-deficient BMSCs. Using quinacrine and LysoTracker, which label vesicular ATP and lysosomal vesicles, respectively (Cao et al., 2014; Huang et al., 2014), we compared vesicular ATP levels between control and

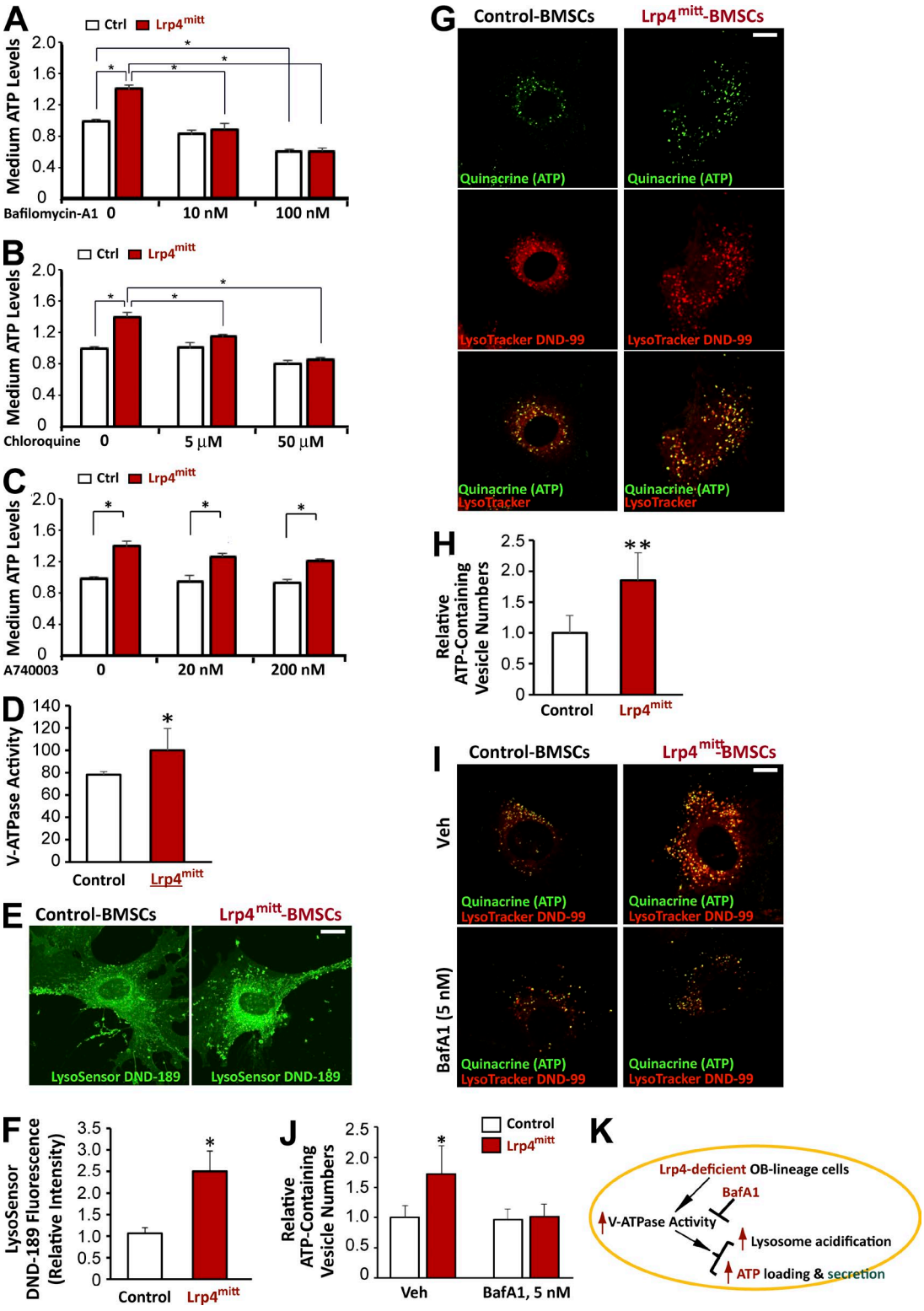

Figure 7. **Elevated v-ATPase–driven vesicular ATP loading and release in Lrp4-deficient OB-lineage cells.** (A–C) Primary cultured WT and Lrp4-deficient BMSCs were treated with sham (PBS), BafA1, chloroquine, or A740003 at the indicated dose. After 2-h treatment, ATP levels in the culture medium were measured using a bioluminescence detection kit. Mean ± SD values from three different experiments are shown. *, $P < 0.05$. (D) Increased V-ATPase activity in Lrp4-deficient BMSCs. Mean ± SD values from experiments using three different preparations are shown. *, $P < 0.05$. (E and F) Increased vesicular acidification in Lrp4-deficient BMSCs. The green fluorescence intensity of LysoSensor was measured by ImageJ (mean ± SD; $n = 20$). Bar, 10 µm. *, $P < 0.05$. (G and H) Increased ATP loading in Lrp4-deficient BMSCs. ATP-containing vesicles were labeled with quinacrine (green channel), and lysosomes were stained with LysoTracker DND-99 (red channel). Bar, 10 µm. Quantification analysis is shown in H. Mean ± SD, $n = 20$; **, $P < 0.001$. (I and J) Primary cultured WT and Lrp4-deficient BMSCs were treated with 5 nM bafilomycin A1 (BafA1) for 1 h. Quinacrine and LysoTracker DND-99 were added. Fluorescence microscopy was undertaken to monitor quinacrine and LysoTracker staining. Bar, 10 µm. Quantification analysis is shown in J. Mean ± SD, $n = 20$; *, $P < 0.05$. (K) Illustration of a working model in which Lrp4 deficiency in OB-lineage cells increases V-ATPase activity, consequently enhancing vesicular ATP loading and release.

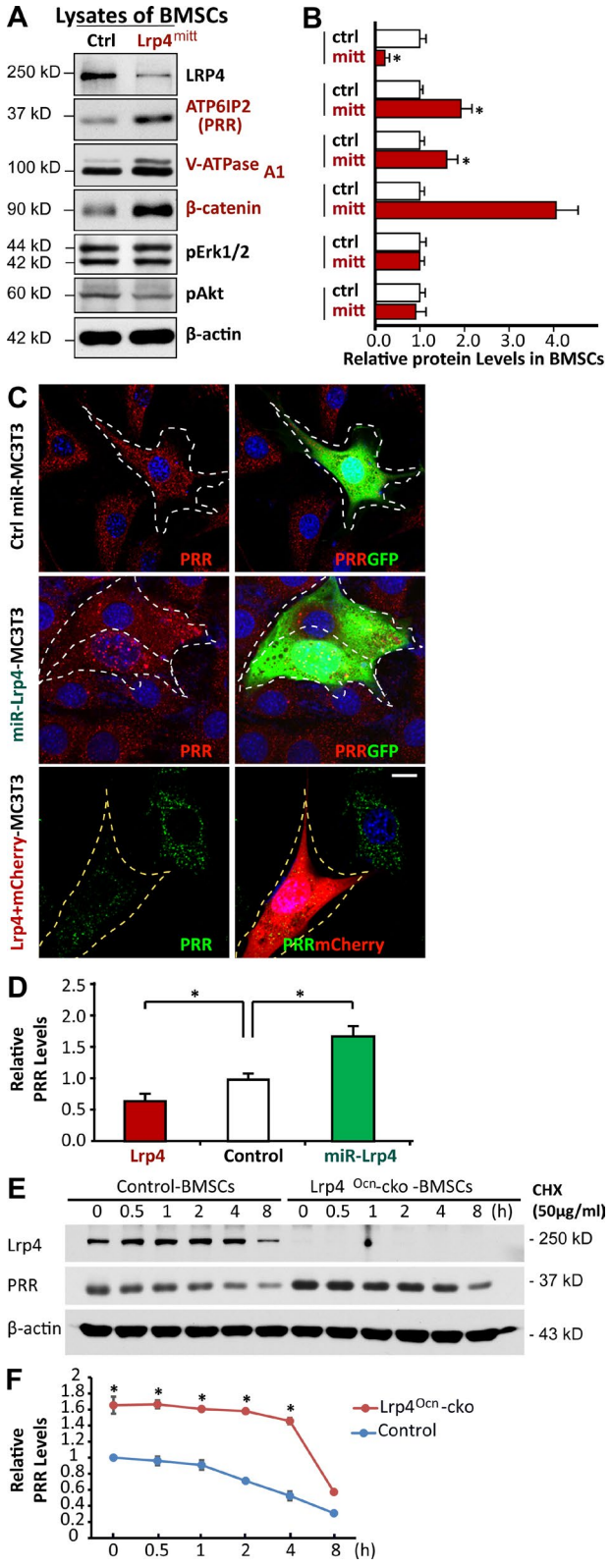

Figure 8. **Increased PRR protein stability in Lrp4-deficient OB-lineage cells.** (A and B) Western blot analysis of indicated protein expression in BMSCs derived from 1-mo-old control and mr-Lrp4^{mitt} mice. Quantification analysis (mean ± SD; n = 3) is presented in B. *, $P < 0.05$. (C and D) Immunostaining analysis of PRR in MC3T3 cells transfected with the indicated plasmids. Representative images are shown in C. Transfected cells are marked with a white dotted line. Bar, 10 µm. Quantification analysis (mean ± SD, n = 20 cells from three different assays; *, $P < 0.05$) is shown in D. (E and F) Time-course analysis of PRR protein levels after cycloheximide (CHX) treatment. Primary cultured BMSCs from 3-mo-old control and Lrp4^{Ocn}-cko mice were treated with 50 µg/ml CHX for the indicated time. PRR protein levels were analyzed by Western blotting. Representative blots are shown in E, and quantification analysis (mean ± SD from three separate experiments; *, $P < 0.05$) is presented in F.

Lrp4-deficient BMSCs. The quinacrine signal was largely colocalized with LysoTracker in both control and Lrp4-deficient BMSCs (Fig. 7 G), in line with studies of ATP in lysosomal vesicles (Cao et al., 2014; Huang et al., 2014). More quinacrine-labeled ATP vesicles were detected in Lrp4-deficient BMSCs than in control cells (Fig. 7, G and H), indicating elevated vesicular ATP loading. Similar results were also detected in Lrp4-deficient OBs (Fig. S3, B–D). Moreover, both quinacrine-ATP and LysoTracker fluorescence signals were V-ATPase activity dependent, as treatment with 5 nM BafA1 largely reduced their fluorescence (Fig. 7, I and J). Together, these results support a working model (Fig. 7 K) in which Lrp4 deficiency in OB-lineage cells increases V-ATPase activity and thus enhances vesicular ATP loading and release.

PRR in ATP release from Lrp4-deficient OB-lineage cells

PRR, also known as ATPase H^+-transporting lysosomal accessory protein 2 (ATP6AP2), is an accessory subunit of the V-ATPase (Cruciat et al., 2010; Ichihara, 2012; Rousselle et al., 2014; Trepiccione et al., 2016). To understand how osteoblastic Lrp4 regulates V-ATPase, we compared their levels in control and Lrp4-deficient BMSCs. Remarkably, levels of both PRR and V-ATPase A1 were higher in Lrp4-deficient BMSCs than in those of controls (Fig. 8, A and B). The PRR increase was also detected in Lrp4-deficient OBs (not depicted) and MC3T3 cells (an OB cell line), whose Lrp4 expression was suppressed by miRNA (Fig. 8, C and D). The increase in PRR or V-ATPase A1 levels was not caused by altered transcription, as their mRNA levels were similar in mutant and control cells (Fig. S4, A and B), implicating a posttranscriptional regulation. Indeed, PRR appeared to be more stable in Lrp4-deficient BMSCs, with a half-life of ∼4 h, twice longer than that of control cells (Fig. 8, E and F). We further examined PRR levels in MC3T3 cells overexpressing Lrp4. The PRR fluorescence signal was lower in cells expressing exogenous Lrp4 than in untransfected cells (Fig. 8, C and D). These results suggest that Lrp4 in OB-lineage cells is necessary and sufficient for PRR down-regulation or degradation.

To determine if increased PRR levels enhance ATP loading and release, MC3T3 cells were transfected with PRR and mCherry. In MC3T3 cells that were positive for exogenous PRR, there was stronger signal of quinacrine staining, compared with untransfected cells or cells transfected with control vector (Fig. 9, A and B), suggesting that a high level of PRR is associated with vesicular ATP loading. In accord, acidification was increased in these cells (Fig. 9, A and C). Next, we infected MC3T3 cells with lentiviral particles encoding shRNA-PRR, which was able to reduce PRR level in infected cells (Fig. S4, C and D). Reducing PRR levels in MC3T3 cells reduced quinacrine staining when compared with control cells (Fig. 9, D and E), indicating compromised vesicular ATP loading. The shRNA-PRR viral infection of Lrp4-deficient BMSCs also reduced ATP level in the CM (Fig. 9, F and G),

and the CM was less effective in causing OC genesis deficits (Fig. 9, H–J). Collectively, these results demonstrate that PRR is necessary and sufficient for vesicular ATP loading and release, revealing a mechanism of elevated ATP release in Lrp4-deficient OB-lineage cells.

Critical role of the interaction between Lrp4 and PRR in Lrp4 down-regulation of PRR and V-ATPase activity

To understand how Lrp4 down-regulates PRR, we first determined whether the two proteins form a complex. HEK293 cells were transfected with Flag-Lrp4 and V5-PRR, and cell lysates were subjected to precipitation with anti-Flag antibody. PRR was detected in precipitates by anti-Flag antibody, but not those precipitated by a nonspecific IgG, suggesting PPR and Lrp4 may form a complex (Fig. S5). To map the domain in Lrp4 to interact with PPR, HEK293 cells were transfected with V5-PRR and a series of Lrp4 deletion mutants (Fig. 10, A and B). As with full-length Lrp4, its extracellular domain was required and sufficient to coimmunoprecipitate with V5-PRR (Fig. 10 B). The interaction was not altered by deleting LDLa (LDLR-A) or the β1 propeller domain, suggesting that these regions are not necessary for interaction. However, deleting β1234 (LDLR-B) or the β12 propeller domains abolished Lrp4's interaction with PRR (Fig. 10 B). These results indicate a role of the β12 propeller domains in forming a complex with PRR.

It is of interest to note that syndactyly cattle or teeth abnormality patients possess two point mutations, G907R and L953P, in the β2 propeller domain (Drögemüller et al., 2007; Khan et al., 2013). Interestingly, L953P mutation reduced the interaction with PRR when compared with WT Lrp4 (Fig. 10 C). Next, we determined whether the Lrp4 interaction is critical for PRR stability. Full-length Lrp4, when expressed in MC3T3 cells, reduced endogenous PRR; in contrast, this effect was not observed in Lrp4 mutants that are unable to interact with PRR (including Lrp4Δβ12, ΔLDLR-B, or L953P; Fig. 10 A, D, and F; and not depicted). Consistently, the expression of Lrp4 in MC3T3 cells also decreased vesicular ATP loading; this effect was undetectable in MC3T3 cells expressing Lrp4 mutants unable to interact with PRR (e.g., Lrp4Δβ12 and L953P; Fig. 10, A, E, and G). These results indicate that Lrp4 suppresses vesicular ATP loading and release by interacting with and thus down-regulating PRR.

Discussion

In this paper, we investigated the molecular mechanism by which osteoblastic Lrp4 regulates OC genesis and function. We found first that Lrp4 deficiency in OB-lineage cells increased the PRR/V-ATPase activity and vesicular ATP release, elevating levels of PPi and adenosine in the extracellular compartment. Second, both pharmacological blocking and genetic ablating $A_{2A}R$ diminished the OC genesis deficit in Lrp4 mutant mice, demonstrating a critical role for adenosine-$A_{2A}R$ signaling in the inhibition of OC genesis. Third, Lrp4 interacted with PRR and was necessary for PRR degradation. These results support a working model depicted in Fig. 10 H, where Lrp4 in OB-lineage cells promotes OC genesis and bone resorption by controlling PRR/V-ATPase–driven vesicular ATP release and thus maintaining extracellular levels of ATP and its derivative, adenosine.

When Lrp4 is mutated in OB-lineage cells, the PRR level is increased, which enhances vesicular ATP loading and release and levels of PPi and adenosine in the extracellular compartment. We propose that adenosine-$A_{2A}R$ signaling may underlie impaired OC genesis via osteoblastic Lrp4 deficiency for the following reasons. First, inhibition of $A_{2A}R$ signaling by its antagonist, SCH58261, but not A740003, an antagonist of ATP-P_2X_7R, was capable of restoring OC genesis and bone resorption in Lrp4 mutant mice (Figs. 3, 4, and S2). Second, knocking out $A_{2A}R$ in Lrp4 mutant mice diminished the OC genesis deficits and restored RANK levels and RANK-mediated OC differentiation (Figs. 5 and 6). Third, the idea that adenosine-$A_{2A}R$ signaling suppresses OC genesis and function is also in line with the previous findings that activation of $A_{2A}R$ by agonist CGS21680 inhibits OC differentiation and function in culture and in vivo (Mediero et al., 2012, 2013), inhibiting $A_{2A}R$ enhances RANKL-induced OC genesis (Mediero and Cronstein, 2013), and $A_{2A}R$ mutant mice exhibit marked reduction in bone density, with increased number and function of $TRAP^+$ OCs (Mediero et al., 2012, 2013). Fourth, although the level of PPi, an inhibitor of OC genesis, was increased in Lrp4-deficient OB-lineage cells, the presence of abundant tissue-nonspecific alkaline phosphatase or alkaline phosphatase in bone tissue (Orimo, 2010; Narisawa et al., 2013) may prevent its accumulation and inhibitory effect in Lrp4 mutant mice. In line with this view, serum levels of PPi are unchanged in Lrp4 mutant mice (Fig. S1 D), and PPi's inhibitory effect on bone mineralization (Nishikawa et al., 1996; Baron et al., 2011; Burr and Russell, 2011; Russell, 2011) is undetectable in Lrp4 mutant mice (Leupin et al., 2011; Chang et al., 2014; Xiong et al., 2015). Finally, other adenosine receptors, such as A_1R, $A_{2B}R$, and A_3R, are unlikely to inhibit OC genesis and function (Mediero and Cronstein, 2013). In contrast, activation of A_1R increases OC genesis and function (Mediero and Cronstein, 2013).

In addition to adenosine-$A_{2A}R$ signaling, the mechanisms of OC genesis deficits in Lrp4 mutant mice may be complex. We previously detected a reduced RANKL/OPG ratio in mr-$Lrp4^{mitt}$ and $Lrp4^{Ocn}$-cko mutant mice, which may also impair OC genesis and bone resorption (Xiong et al., 2015). The results presented in Fig. 1 (F and G) suggest a delayed RANKL-induced in vitro OC differentiation in BMMs from Lrp4 mutant mice, which do not exclude RANKL/OPG's contribution in vivo. In fact, the partial rescue of the bone resorption in Lrp4 mutant mice by inhibition of $A_{2A}R$ (Figs. 4 F and 5 E) suggest that additional factors are involved in this event. Furthermore, increased DKK1 in Lrp4 mutant mice may also inhibit OC genesis by inhibiting Wnt5a-induced OC genesis (Baron and Kneissel, 2013). These alternative mechanisms warrant additional investigation.

Intriguingly, blocking P_2X_7R (by A740003), a primary receptor of ATP, diminished overgrowth of bone mass in Lrp4 mutant mice (Fig. S2), suggesting a potential involvement of ATP activation of P_2X_7R in eventual phenotype manifestation. However, A740003 did not increase the number of $TRAP^+$ cells or elevate bone resorption in $Lrp4^{Ocn}$-cko mice (Fig. S2, F–H). Instead, serum Ocn levels were reduced in A740003-treated mice (Fig. S2 I). These observations suggest that the ATP-P_2X_7R pathway may promote OB-mediated bone formation instead of OC-mediated bone resorption.

PRR appears to be a multifunctional protein. It was initially identified as a PRR critical for renin signaling and function (Nguyen, 2011). It is also an important component of V-ATPase

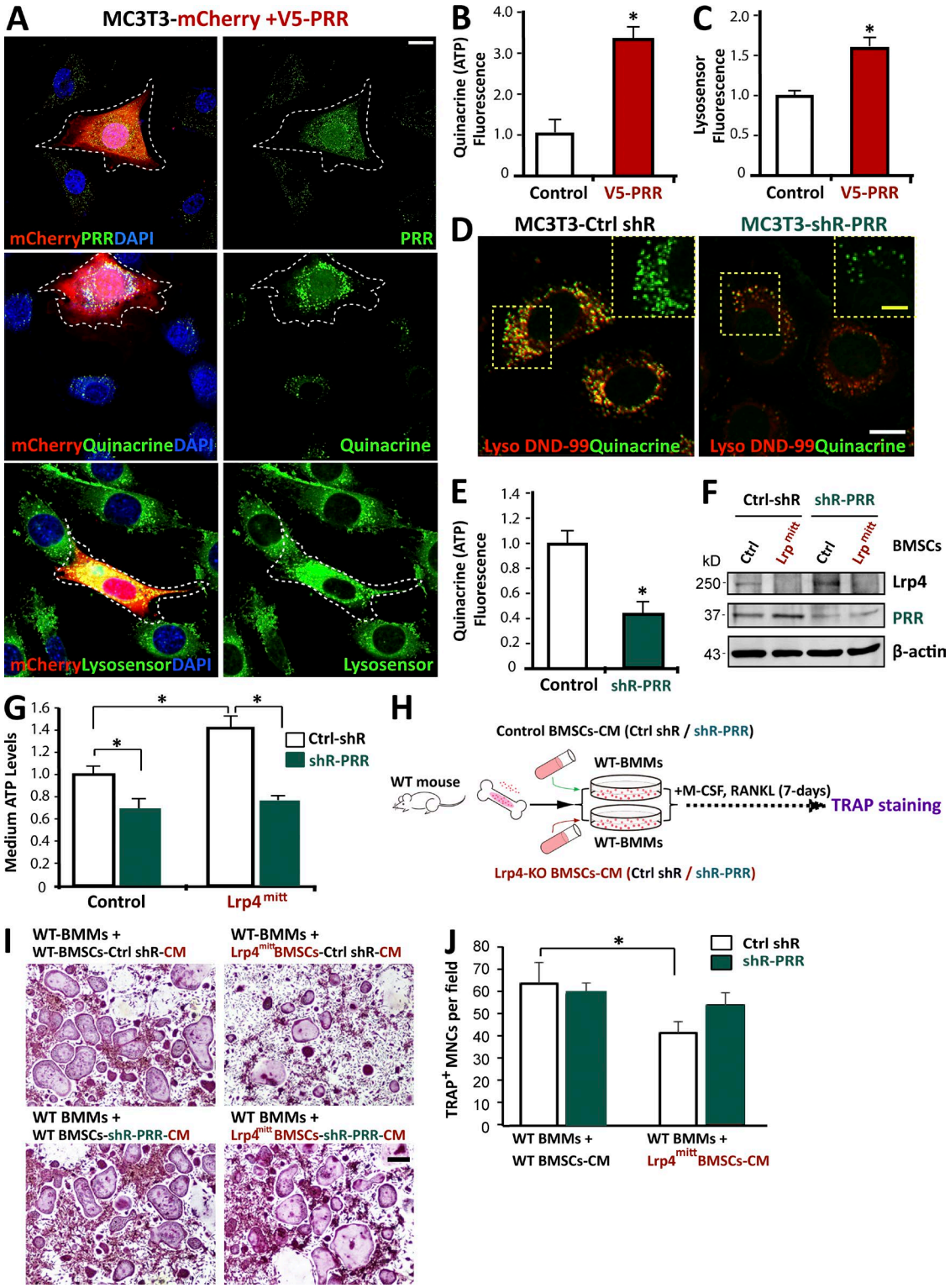

Figure 9. **PRR is critical for ATP release from Lrp4-deficient OB-lineage cells.** (A–C) Increased ATP loading and vesicular acidification in MC3T3 cells expressing V5-PRR. ATP-containing vesicles were labeled with quinacrine. The green fluorescent intensity of LysoSensor was measured by Image J (mean ± SD; *n* = 20). Quantification analysis is shown in B and C. Bar, 10 µm. *, P < 0.05. (D and E) Decreased ATP loading in MC3T3 cells suppressing PRR. Cells were costained with LysoTracker DND-99 and quinacrine. White bar, 10 µm; and yellow bar, 5 µm. Quantification analysis is shown in E. Mean ± SD, *n* = 20; *, P < 0.05. (F) Western blot analysis of Lrp4 and PRR expression in control and PRR-KD BMSCs. BMSCs derived from 1-mo-old control and mr-Lrp4^{mitt} mice were infected with control and shR-PRR lentiviruses. The cell lysates were subjected to the Western blot analysis using indicated antibodies. (G) Medium ATP levels in PRR-KD BMSCs. The values of mean ± SD from three different experiments were presented. *, P < 0.05. (H) Experimental strategy. TRAP staining of WT BMMs that were treated with CM of control or PRR-KD BMSCs. (I and J) TRAP staining analysis of OC cultures that were treated with CM plus RANKL for 7 d. Representative images are shown in I. Bar, 150 µm. Quantitative analysis of TRAP^{+} multinuclei cells (MNCs) per field is presented in J. Mean ± SD values from three different cultures are shown. *, P < 0.05.

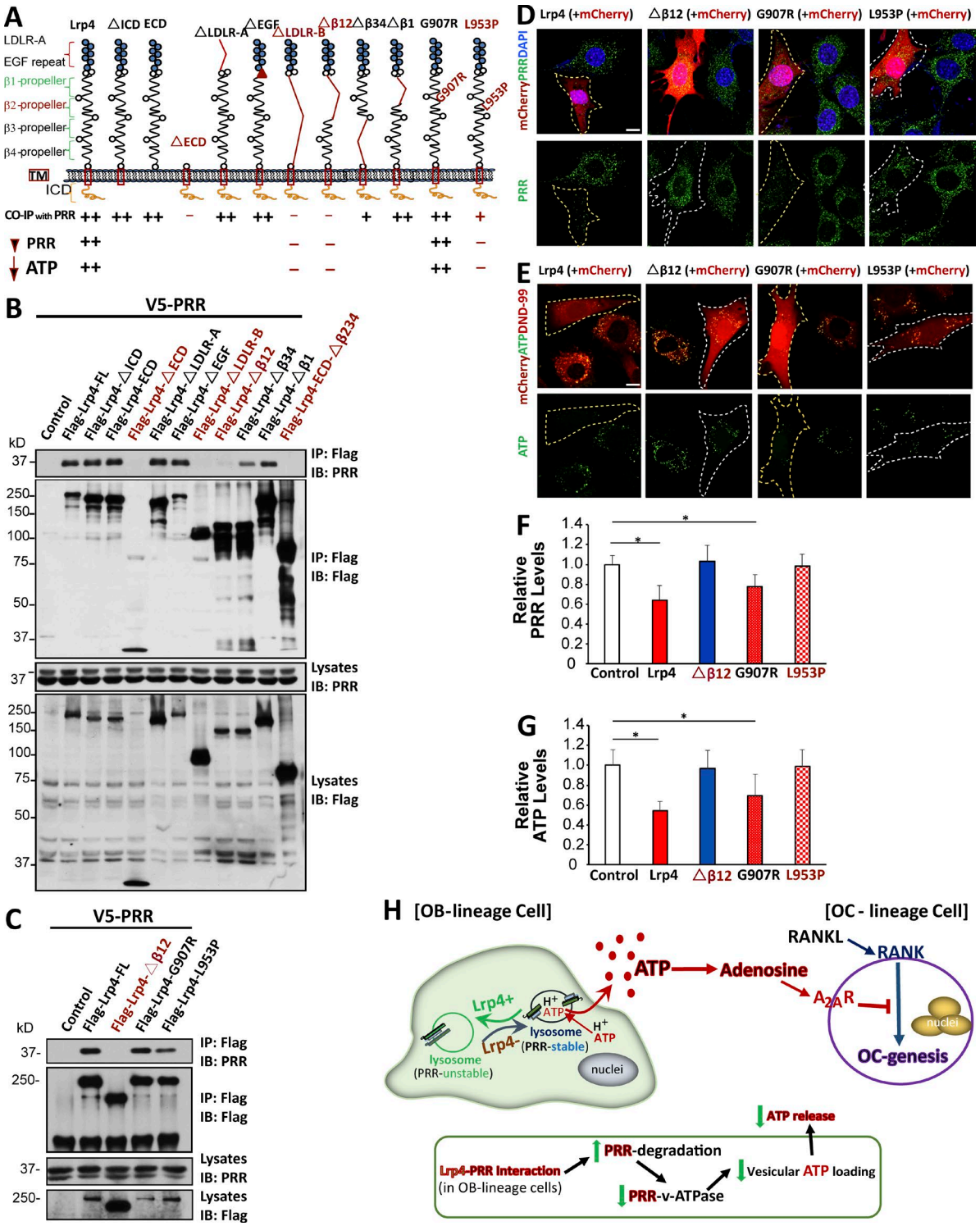

Figure 10. **Critical role of Lrp4's interaction with PRR in Lrp4's down-regulation of PRR and V-ATPase activity.** (A) Illustration of various deletion mutants of Lrp4. (B and C) Coimmunoprecipitation analysis of Lrp4 and its mutant with PRR. HEK293T cells were transfected with the indicated plasmids. 48 h after transfection, ~500 µg cell lysates was immunoprecipitated by anti-Flag M2-agarose. The resulting lysates were subjected to Western blot analysis using indicated antibodies. Approximately 50 µg cell lysates was used as an input. Data presented are representative of three independent experiments. (D and F) Effects of Lrp4 and its mutant on PRR levels in MC3T3 cells. MC3T3 cells transfected with mCherry plus Flag-Lrp4, Flag-Lrp4-dβ12, Flag-Lrp4-G907R, or Flag-Lrp4-L953P were fixed and immunostained with anti–PRR antibody. Representative images are shown in D. Transfected cells are marked with white line. Bar, 10 µm. Quantification analysis of data from D is shown in F. Mean ± SEM values (n = 20 cells from three different assays) are presented. *, $P < 0.05$. (E and G) Effects of Lrp4 and its mutant on ATP loading in MC3T3 cells. Bar, 10 µm. Quantification analysis is shown in G; mean ± SD; n = 20. *, $P < 0.05$. (H) Illustration of a working model. Lrp4 deficiency in OB-lineage cells increases PRR-associated V-ATPase activity in lysosomes, thus promoting vesicle H^+ gradient and acidification, accelerates vesicular ATP release, and elevates extracellular adenosine production, which inhibits OC genesis.

(Nguyen, 2011; Ichihara, 2012; Rousselle et al., 2014; Trepiccione et al., 2016). Studies indicate that ATP release from OBs is primarily mediated by vesicular exocytosis (Genetos et al., 2005; Orriss et al., 2009, 2013; Burnstock et al., 2013), which depends on the V-ATPase activity (Rudnick, 2008; Burnstock et al., 2013). Lrp4 deficiency in OB-lineage cells increases PRR-associated V-ATPase activity in endosomes and lysosomes and thus promotes vesicle H^+ gradient and acidification and accelerates vesicular ATP release (Fig. 10 H). Recently, PRR/V-ATPase has been shown to regulate Wnt–β-catenin signaling (Buechling et al., 2010; Cruciat et al., 2010). PRR interacts with the Wnt receptors LRP6 and frizzled in HEK293 cells, *Xenopus laevis* tadpoles, and *Drosophila melanogaster* (Buechling et al., 2010; Cruciat et al., 2010). Genetic inhibition of PRR or pharmacological inactivation of V-ATPase reduces Wnt canonical (β-catenin) and noncanonical (planar cell polarity) signaling (Buechling et al., 2010; Cruciat et al., 2010). In contrast, Lrp4 may act as a sclerostin receptor, which could inhibit Wnt–β-catenin signaling (Leupin et al., 2011; Chang et al., 2014; Xiong et al., 2015; Fijalkowski et al., 2016). Therefore, PRR/V-ATPase may be a convergence point for multiple pathways regulating bone homeostasis.

Materials and methods

Reagents and animals

Rabbit polyclonal antibodies, including PRR (HPA003156; Sigma-Aldrich), V-ATPase A1 (sc-28801; Santa Cruz Biotechnology, Inc.), pErk1/2 (4370S; Cell Signaling Technology), pAkt (4060P; Cell Signaling Technology), c-Fms (M-CSF receptor antibody, #3152; Cell Signaling Technology), adenosine receptor A_{2a} (ab3461; Abcam), and RANK (4845S; Cell Signaling Technology), were used. Mouse monoclonal antibodies, including Lrp4 (ECD) clone N207/27 (75–221; University of California, Davis/National Institutes of Health NeuroMab Facility), Flag (F1804; Sigma-Aldrich), V5 (V8012; Sigma-Aldrich), β-catenin (BD), and β-actin (A1978; Sigma-Aldrich), were used. Rat monoclonal antibodies, including anti-CD11b-FITC (SAB4700582-100UG; Sigma-Aldrich) and PE anti–mouse RANK (119806; BioLegend), were used. Secondary antibodies were purchased from Jackson ImmunoResearch Laboratories, Inc. Cycloheximide solution (C4859), A740003 (A0862), chloroquine (C6628), and quinacrine (Q3251) were obtained from Sigma-Aldrich. SCH58261 was obtained from Tocris Bioscience (2270), and BafA1 was obtained from Abcam (ab120497). LysoSensor Green DND-189 (L-7535) and LysoTracker Red DND-99 (L7528) were obtained from Thermo Fisher Scientific. M-CSF and RANKL were gifts from X. Feng (University of Alabama at Birmingham, Birmingham, AL). Other chemicals and reagents used in this study were of analytical grade.

$Lrp4^{mitt}$ mice were obtained from L.A. Niswander (University of Colorado, Aurora, CO) and generated by using ENU (Weatherbee et al., 2006). Mice were crossed with human skeletal α-actin promotor-driven Cre transgenic mice to generate muscle rescued Lrp4 null allele (mr-$Lrp4^{mitt}$). Generation, crossing, and genotyping of floxed Lrp4 mice were described previously (Wu et al., 2012). The floxed Lrp4 ($Lrp4^{f/f}$) mice were crossed with Ocn-Cre transgenic mice to generate $Lrp4^{Ocn}$-cko mutant mice. The Ocn-Cre mice were provided by T. Clemens (Johns Hopkins Medical School, Baltimore, MD) and X. Shi (Augusta University, Augusta, GA). A_{2A}R-KO mice were obtained from The Jackson Laboratory (stock number 010685). The mutant mice were backcrossed into C57BL/5J mice. All experimental procedures were approved by the Institutional Animal Care and Use Committee at Augusta University, according to National Institutes of Health guidelines.

Plasmids and lentiviruses

Original Lrp4 constructs were gifts from T. Suzuki (Shinshu University, Matsumoto, Japan). To generate Flag-Lrp4 and Flag-Lrp4 mutants, we amplified full-length Lrp4 and mutant Lrp4 cDNA by PCR from the original Lrp4 construct and subcloned the cDNA into pFlag-CMV1 downstream of an artificial signal peptide sequence and a Flag epitope (Wu et al., 2012). G907R (GGA to CGA) and L953P (CTA to CCA) point mutations were made from the Flag-Lrp4 construct using the Phusion High-Fidelity PCR kit (E0553L; New England Biolabs, Inc.) and Restriction Endonucleases DpnI (R0176L; New England Biolabs, Inc.). Lrp4-miRNA construct miLrp4-1062 was generated using the BLOCK-it Pol II miR RNAi expression vector kit (K4936-00; Invitrogen), which has been previously described and verified to be most potent in inhibiting Lrp4 expression (Zhang et al., 2008). V5-PRR plasmid was purchased from DNASU (ATP6AP2 in pLX304, HsCD00446844). Renin receptor shRNA lentiviral particles (shR-PRR) were obtained from Santa Cruz Biotechnology, Inc. (sc-62935-V). The authenticity of all constructs was verified by DNA sequencing.

In vitro OB/OC lineage cell culture

Whole bone marrow cells were flushed from long bones of WT and Lrp4-deficient mice and plated on 100-mm culture plates in DMEM containing 1% penicillin/streptomycin (P/S) and 10% FBS for 2 d. For OB-lineage culture, plates with adherent cells were replaced with fresh culture medium every 3 d. After 7 d of passaging by trypsin digestion, $1 \times 10^4/cm^2$ BMSCs were plated for experiments. For OC lineage culture, nonadherent cells were harvested and subjected to Ficoll-Hypaque gradient centrifugation for purification of BMMs. Cells were plated on 100-mm culture dishes in α-MEM containing 10% FBS, 1% P/S, and 10 ng/ml recombinant M-CSF.

For osteoclastogenesis, 5×10^4 BMMs were incubated with OC differentiation medium containing 10 ng/ml recombinant M-CSF and 100 ng/ml recombinant RANKL. Mature OCs began to form at day 4 to 5 after RANKL treatment. The cells were then subjected to TRAP staining to confirm their OC identity.

For CM treatment, BMSCs were plated on 100-mm tissue culture plates in α-MEM containing 10% FBS and 1% P/S. BMMs derived from WT mice were placed onto presterilized glass coverslips on 12-well plates. CM from OB-lineage cells plates plus 10 ng/ml recombinant M-CSF and 100 ng/ml recombinant RANKL were added to 12-well plates containing BMM every day. After 7 d, cells were subjected to TRAP staining.

Primary OB cultures were prepared from long bones of 1-mo-old WT/mr-$Lrp4^{mitt}$ or 3-mo-old Ocn-Cre/$Lrp4^{Ocn}$-cko mice. In brief, small bone pieces were incubated in collagenase solution to remove all remaining soft tissue and adhering cells and then transferred to 60-mm culture dishes containing DMEM medium supplemented with 10% FBS, 1% P/S, 10 mM β-glycerophosphate, and 50 µM L-ascorbic acid-2-phosphate. Culture medium was replaced three times per week. Bone cells started to migrate from the bone chips after 3–5 d. After 2 wk, the monolayer was trypsinized by incubating the cells with trypsin solution.

Cell lines and transfection

MC3T3-E1 or HEK293 cells were maintained in DMEM supplemented with 10% FCS and 1% P/S. For transient transfection, MC3T3-E1 cells were plated at a density of 10^6 cells per 10-cm culture dish and allowed to grow for 12 h before transfection using a Lipofectamine 3000 Transfection kit (L3000; Invitrogen). 48 h after transfection, cells were

subjected to immunostaining analysis. HEK293 cells were transfected by polyethylenimine (PEI), as described previously (Xia et al., 2013; Xiong et al., 2015). In brief, 12 µg DNA mixture was prepared in serum-free DMEM, 6 µl PEI (based on a 3:1 ratio of PEI/total DNA) was added to the diluted DNA and mixed immediately by pipetting. After incubation for 20 min at room temperature, the DNA/PEI mixture was added to cells, and 48 h later, transfected cells were subjected to Western blot or coimmunoprecipitation assay.

The PRR-KD cell line or PRR-KD BMSCs were obtained by infection of MC3T3-E1 cells or BMSCs with lentiviral particles encoding scramble control or shRNA-PRR, respectively. In brief, cells were infected with the lentiviral particles for 1 d in 2 µg/ml polybrene medium. At day 3, the culture medium was removed and replaced with complete medium (without polybrene). After 5–6 d, stable clones expressing the shRNA were selected via 5 µg/ml puromycin dihydrochloride, which induces death of untransduced cells.

FACS analysis

FACS was performed as described previously (Xia et al., 2013). In brief, BMMs derived from 3-mo-old OcnCre, Lrp4^{Ocn}-cko, A_{2A}R-KO, and Lrp4^{Ocn}-cko;A_{2A}R-KO mice were resuspended in ice-cold PBS. PE-RANK and FITC-CD11b antibodies (0.1–10 µg/ml) were added into the tube and incubated for at least 30 min at 4°C in the dark. The cells were washed three times with ice-cold PBS (with 0.5% PFA) and then immediately subjected to FACS analysis at the core facility (Augusta University).

Measuring levels of ATP, PPi, adenosine, SOST, and Wise

ATP levels were measured using a bioluminescence detection kit (FF2000; Promega) according to the manufacturer's instructions. In brief, CMs or cell lysate samples were incubated with the ectonucleotidase inhibitor ARL 67165 trisodium salt hydrate (A265; Sigma-Aldrich) to inhibit ATP hydrolysis. ATP was measured by a luciferase reaction in which 560-nm light was emitted when D-luciferin was converted to oxyluciferen. Luminescence was measured using a luminometer (TR717; PE Applied Biosystems). ATP was calculated based on a calibration curve with standard samples. Total cell protein in each well was used for normalization.

PPi and adenosine levels were measured using fluorometric assay kits (pyrophosphate assay kit, ab179836, Abcam; and adenosine assay kit, K327-100; BioVision, Inc.). SOST and Wise levels were measured by ELISAs (mouse/rat SOST Microplate, MSST00; R&D Systems; and enzyme-linked immunosorbent assay kit for SOSTDC1, SEF900Mu; Cloud-Clone Corp).

Measurement of mitochondrial capacity using the Seahorse platform

OCR was analyzed in an X96 Extracellular Flux Analyzer with XF Cell Mito Stress Test kit (Seahorse Biosciences) at 37°C. OBs isolated from OcnCre and Lrp4^{Ocn}-cko mice were plated on XF96 cell culture plates at 40,000 per well and cultured for 3 d. As temperature and background controls, four wells without OB seeding from each plate were set. For measurement, OBs were gently rinsed with 100 µl/well XF Base medium with 2 mM glutamine and 10 mM glucose. 175 µl/well fresh assay medium was added and assayed. The ATP synthase inhibitor oligomycin, the mitochondrial uncoupler carbonyl FCCP, and the complex I inhibitor rotenone were sequentially injected, and three baseline recordings were made. OCR measurements were performed at 3-min intervals, and each condition was measured in an independent well.

Cell lysis, Western blot, and coimmunoprecipitation

Cells were lysed in lysis buffer containing 50 mM Tris-HCl, pH 7.5, 150 mM NaCl, 1% (vol/vol) Triton X-100, 0.1% SDS, 0.5% deoxycholate, and 1 mM EDTA, supplemented with protease inhibitors (1 µg/ml leupeptin and pepstatin, 2 µg/ml aprotinin, and 1 mM PMSF) and phosphatase inhibitors (10 mM NaF and 1 mM Na_3VO_4). Whole-cell extracts were fractionated by SDS-PAGE and transferred to a nitrocellulose membrane (Bio-Rad Laboratories). After incubation with 5% milk in TBST (10 mM Tris, 150 mM NaCl, and 0.5% Tween 20, pH 8.0) for 1 h, the membrane was incubated with indicated antibodies overnight at 4°C. Membranes were washed with TBST three times and incubated with a 1:5,000 dilution of horseradish peroxidase–conjugated anti–mouse or anti–rabbit antibodies for 1 h. Blots were washed with TBST three times and developed with the ECL system (Bio-Rad Laboratories). Immunoprecipitation was performed with an anti-Flag antibody or anti-Flag M2 Agarose (Sigma-Aldrich). Western blotting was performed using the ECL procedure, according to the manufacturer's instructions (Bio-Rad Laboratories), with a mouse monoclonal Flag antibody to detect the coimmunoprecipitation of Flag-Lrp4 or anti-V5 monoclonal antibody or anti–PRR rabbit polyclonal antibody for PRR proteins.

Immunofluorescence staining and imaging analysis

To image ATP loading, cells were incubated with 5 µM quinacrine and 50 nM LysoTracker Red DND-99 for 30 min at 37°C. Images were acquired using a confocal microscope (ZEN software; ZEISS) by sequential excitation at 488 nm for quinacrine and 543 nm for LysoTracker. To measure vesicular acidification, cells were treated with 1 µM LysoSensor Green DND-189 for 30 min. Images were acquired using a confocal microscope by excitation at 488 nm.

For immunofluorescence staining, cells on coverslips were fixed with 4% paraformaldehyde at room temperature for 20 min, permeabilized with 0.15% Triton X-100 for 8 min, and then subjected to coimmunostaining analysis using indicated antibodies. Stained cells were washed three times with PBS and mounted with VECTASHIELD (H-1500; Vector Laboratories) and imaged by confocal microscope at room temperature. Fluorescent quantification was performed using Zen software according to the manufacturer's instructions (ZEISS).

V-ATPase activity assay

Each sample (20 µg protein) was added to a solution containing 2 mM ATP, 3 mM $MgSO_4$, 25 mM Tris-SO_4, pH 8.0, and 5 mM NaN_3. The samples (with or without 1 µM BafA1 to test V-ATPase specific activity) were incubated at 37°C for 20 min, and the reaction was stopped by the addition of 150 µl solution A (12% SDS). Inorganic phosphate was measured using a modified Chifflet's assay (Chifflet et al., 1988; González-Romo et al., 1992). Different concentrations of K_2HPO_4 (ranging from 0 to 200 µM) were used to generate a standard curve. Solution B (12% ascorbic acid in 1 N HCl and 200 µM EDTA) and solution C (2% ammonium molybdate in 1 N HCl) were combined 1:1 at the time of the experiment (named solution D) and added to each of the samples (300 µl per group). After 3 min, solution E (2% sodium citrate and 2% sodium meta-arsenite in 2% acetic acid in ddH_2O) was then added and allowed in incubate for 20 min at room temperature. Absorbance was read using a spectrophotometer at 850 nM. The color developed was stable up to 5 h. V-ATPase activity was calculated as BafA1-inhibited ATP hydrolysis.

µCT

The µCT analyses were performed as described previously (Xia et al., 2013; Xiong et al., 2015). Excised femurs from mice were scanned using the Scanco µCT40 desktop cone-beam micro-CT scanner (Scanco Medical) using µCT Tomography v5.44. Scans were automatically reconstructed into 2D slices, and all slices were analyzed using the µCT Evaluation Program (v.6.5-2; Scanco Medical). The femur was placed inverted in a 12-mm-diameter scanning holder and scanned at the following settings: 12 µm resolution, 55 kVp, and 145 µA with

an integration time of 200 ms. For the cortical analysis, the bone was scanned at the midshaft of the bone for a scan of 25 slices. The region of interest was drawn on every slice and fitted to the outside of the cortical bone to include all the bone and marrow. The threshold for cortical bone was set at 329. 3D reconstruction (μCT Ray v3.8) was performed using all outlined slices. Data were obtained on BV, total volume (TV), BV/TV, bone density, and cortical thickness. For the trabecular bone, the scan was started at the growth plate and consisted of 211 slices. The region of interest was outlined starting below the growth plate (for the femurs from 1-mo-old mice) and where the condyles ended (for the femurs from older mice). 100 slices were outlined from this point, on the inside of the cortical bone, enclosing only the trabecular bone and marrow. Trabecular bone was thresholded at 245 and the 3D analysis performed on the 100 slices. Data were obtained on BV, density, TV, trabecular number, thickness, and separation.

Bone histomorphometric analysis

Bone histomorphometric analyses were performed as previously described (Xia et al., 2013; Xiong et al., 2015). In brief, mouse tibia and femurs were fixed overnight in 10% formalin, decalcified in 14% EDTA, embedded in paraffin, sectioned, and subjected to hematoxylin and eosin and TRAP staining. Morphometric perimeters were determined by measuring the areas situated at least 0.5 mm from the growth plate, excluding the primary spongiosa and trabeculae connected to the cortical bone.

Measurements of serum levels of Ocn, PYD, and calcium

Blood samples were collected, allowed to clot for 30 min, and centrifuged for 10 min at 3,000 rpm. Serum was frozen at −80°C until use. Ocn, PYD, and calcium were measured in duplicate with an Ocn ELISA kit (Biomedical Technologies, Inc.), a METRA serum PYD RIA kit (Quidel Corporation), and a calcium detection kit (Abcam), respectively, as described previously (Xia et al., 2013; Xiong et al., 2015). Concentrations were obtained by comparing readings against standard curves.

RNA isolation and real time-PCR

Total RNA was isolated by TRIzol extraction (Invitrogen). Quantitative PCR was performed using a Quantitect SYBR Green PCR kit (Bio-Rad Laboratories) with a real-time PCR System (Opticon Monitor 3). The following primers were used: CD39, 5′-ATGCTTTAACCCAGGATA CGA-3′ and 5′-AGGGCAGTGGCTGTTGTT-3′; CD73, 5′-TCCGCA AGGAAGAACCCA-3′ and 5′-GTGCCATAGCATCGTAGCC-3′; PRR, 5′-CAGCGTCATCTCCTACCC-3′ and 5′-ACACCGAGTTTG CTTTCC-3′; V-ATPase, 5′-ACTAAGCAAAGAAGACAGGGAG-3′ and 5′-CACCGACAGCGTCAAACA-3′; RANKL, 5′-ATCCCATCG GGTTCCCATAA-3′ and 5′-TCCGTTGCTTAACGTCATGTTAG-3′; OPG, 5′-GGCCTGATGTATGCCCTCAA-3′ and 5′-GTGCAG GAACCTCATGGTCTTC-3′; β-actin primers (5′-AGGTCATCACTA TTGGCAACGA-3′ and 5′-CATGGATGCCACAGGATTCC-3′) were used for normalization.

Statistical analysis

All data are expressed as mean ± SD. For in vivo studies, five or six mice per genotype per assay were used. For in vitro cell biological and biochemical studies, each experiment was repeated three times. 10–50 cells were quantified for immunostaining analyses. Data were analyzed by Student's *t* test, two-way analysis of variance (ANOVA), and post-hoc test (GraphPad Software Prism 5). The significance level was set at $P < 0.05$.

Online supplemental material

Fig. S1 shows that ATP levels were increased in CMs of Lrp4-deficient BMSCs. Fig. S2 demonstrates trabecular bone loss in $Lrp4^{Ocn}$-cko mice by A740003, an antagonist of P_2X_7R. Fig. S3 shows elevated v-ATPase–driven vesicular ATP loading and release in Lrp4-deficient OBs. Fig. S4 shows unchanged expression levels of PRR in Lrp4-deficient BMSCs and MC3T3 cells. Fig. S5 demonstrates the interaction of Lrp4 with PRR.

Acknowledgments

We thank Ms. Xue-Mei Cao (University of Alabama at Birmingham) for μCT analysis and members of the Xiong and Mei laboratories for helpful discussions. We thank Drs. X. Feng, X.M. Shi, T. Clemens, and T. Suzuki for providing reagents.

This study was supported in part by grants from the National Institutes of Health (to W.-C. Xiong and L. Mei) and the U.S. Department of Veterans Affairs (to W.-C. Xiong).

The authors declare no competing financial interests.

Author contributions: W.-C. Xiong and L. Xiong designed research. L. Xiong performed the experiments shown in Figs. 1–10, and J.-U. Jung performed the experiments shown in Fig. 1. H.-H. Guo and J.-X. Pan assisted in primary cell cultures and bone histomorphometric analysis. X.-D. Sun assisted in ATP measurements. W.-C. Xiong, L. Xiong, and L. Mei analyzed data. W.-C. Xiong, L. Mei, and L. Xiong wrote the paper.

Submitted: 1 August 2016
Revised: 23 November 2016
Accepted: 10 January 2017

References

Ahn, Y., C. Sims, J.M. Logue, S.D. Weatherbee, and R. Krumlauf. 2013. Lrp4 and Wise interplay controls the formation and patterning of mammary and other skin appendage placodes by modulating Wnt signaling. *Development.* 140:583–593. http://dx.doi.org/10.1242/dev.085118

Balemans, W., N. Patel, M. Ebeling, E. Van Hul, W. Wuyts, C. Lacza, M. Dioszegi, F.G. Dikkers, P. Hildering, P.J. Willems, et al. 2002. Identification of a 52 kb deletion downstream of the SOST gene in patients with van Buchem disease. *J. Med. Genet.* 39:91–97. http://dx.doi.org/10.1136/jmg.39.2.91

Bankston, L.A., and G. Guidotti. 1996. Characterization of ATP transport into chromaffin granule ghosts. Synergy of ATP and serotonin accumulation in chromaffin granule ghosts. *J. Biol. Chem.* 271:17132–17138. http://dx.doi.org/10.1074/jbc.271.29.17132

Baron, R., and M. Kneissel. 2013. WNT signaling in bone homeostasis and disease: From human mutations to treatments. *Nat. Med.* 19:179–192. http://dx.doi.org/10.1038/nm.3074

Baron, R., S. Ferrari, and R.G. Russell. 2011. Denosumab and bisphosphonates: Different mechanisms of action and effects. *Bone.* 48:677–692. http://dx.doi.org/10.1016/j.bone.2010.11.020

Bowman, E.J., A. Siebers, and K. Altendorf. 1988. Bafilomycins: A class of inhibitors of membrane ATPases from microorganisms, animal cells, and plant cells. *Proc. Natl. Acad. Sci. USA.* 85:7972–7976. http://dx.doi.org/10.1073/pnas.85.21.7972

Buechling, T., K. Bartscherer, B. Ohkawara, V. Chaudhary, K. Spirohn, C. Niehrs, and M. Boutros. 2010. Wnt/Frizzled signaling requires dPRR, the *Drosophila* homolog of the prorenin receptor. *Curr. Biol.* 20:1263–1268. http://dx.doi.org/10.1016/j.cub.2010.05.028

Burnstock, G., T.R. Arnett, and I.R. Orriss. 2013. Purinergic signalling in the musculoskeletal system. *Purinergic Signal.* 9:541–572. http://dx.doi.org/10.1007/s11302-013-9381-4

Burr, D., and G. Russell. 2011. Foreword: Bisphosphonates. *Bone.* 49:1. http://dx.doi.org/10.1016/j.bone.2011.05.019

Cao, Q., K. Zhao, X.Z. Zhong, Y. Zou, H. Yu, P. Huang, T.L. Xu, and X.P. Dong. 2014. SLC17A9 protein functions as a lysosomal ATP transporter and regulates cell viability. *J. Biol. Chem.* 289:23189–23199. http://dx.doi.org/10.1074/jbc.M114.567107

Chang, M.K., I. Kramer, T. Huber, B. Kinzel, S. Guth-Gundel, O. Leupin, and M. Kneissel. 2014. Disruption of Lrp4 function by genetic deletion or pharmacological blockade increases bone mass and serum sclerostin levels. *Proc. Natl. Acad. Sci. USA.* 111:E5187–E5195. http://dx.doi.org/10.1073/pnas.1413828111

Chen, P.M., Z.J. Gombart, and J.W. Chen. 2011. Chloroquine treatment of ARPE-19 cells leads to lysosome dilation and intracellular lipid accumulation: Possible implications of lysosomal dysfunction in macular degeneration. *Cell Biosci.* 1:10. http://dx.doi.org/10.1186/2045-3701-1-10

Chifflet, S., A. Torriglia, R. Chiesa, and S. Tolosa. 1988. A method for the determination of inorganic phosphate in the presence of labile organic phosphate and high concentrations of protein: Application to lens ATPases. *Anal. Biochem.* 168:1–4. http://dx.doi.org/10.1016/0003-2697(88)90002-4

Choi, H.Y., M. Dieckmann, J. Herz, and A. Niemeier. 2009. Lrp4, a novel receptor for Dickkopf 1 and sclerostin, is expressed by osteoblasts and regulates bone growth and turnover in vivo. *PLoS One.* 4:e7930. http://dx.doi.org/10.1371/journal.pone.0007930

Coco, S., F. Calegari, E. Pravettoni, D. Pozzi, E. Taverna, P. Rosa, M. Matteoli, and C. Verderio. 2003. Storage and release of ATP from astrocytes in culture. *J. Biol. Chem.* 278:1354–1362. http://dx.doi.org/10.1074/jbc.M209454200

Cruciat, C.M., B. Ohkawara, S.P. Acebron, E. Karaulanov, C. Reinhard, D. Ingelfinger, M. Boutros, and C. Niehrs. 2010. Requirement of prorenin receptor and vacuolar H+-ATPase-mediated acidification for Wnt signaling. *Science.* 327:459–463. http://dx.doi.org/10.1126/science.1179802

Drögemüller, C., T. Leeb, B. Harlizius, I. Tammen, O. Distl, M. Höltershinken, A. Gentile, A. Duchesne, and A. Eggen. 2007. Congenital syndactyly in cattle: Four novel mutations in the low density lipoprotein receptor-related protein 4 gene (LRP4). *BMC Genet.* 8:5. http://dx.doi.org/10.1186/1471-2156-8-5

Fijalkowski, I., E. Geets, E. Steenackers, V. Van Hoof, F.J. Ramos, G. Mortier, A.M. Fortuna, W. Van Hul, and E. Boudin. 2016. A novel domain-specific mutation in a sclerosteosis patient suggests a role of LRP4 as an anchor for sclerostin in human bone. *J. Bone Miner. Res.* 31:874–881. http://dx.doi.org/10.1002/jbmr.2782

Folestad, A., M. Ålund, S. Asteberg, J. Fowelin, Y. Aurell, J. Göthlin, and J. Cassuto. 2015. Role of Wnt/β-catenin and RANKL/OPG in bone healing of diabetic Charcot arthropathy patients. *Acta Orthop.* 86:415–425. http://dx.doi.org/10.3109/17453674.2015.1033606

Fujita, K., and S. Janz. 2007. Attenuation of WNT signaling by DKK-1 and -2 regulates BMP2-induced osteoblast differentiation and expression of OPG, RANKL and M-CSF. *Mol. Cancer.* 6:71. http://dx.doi.org/10.1186/1476-4598-6-71

Genetos, D.C., D.J. Geist, D. Liu, H.J. Donahue, and R.L. Duncan. 2005. Fluid shear-induced ATP secretion mediates prostaglandin release in MC3T3-E1 osteoblasts. *J. Bone Miner. Res.* 20:41–49. http://dx.doi.org/10.1359/JBMR.041009

González-Romo, P., S. Sánchez-Nieto, and M. Gavilanes-Ruíz. 1992. A modified colorimetric method for the determination of orthophosphate in the presence of high ATP concentrations. *Anal. Biochem.* 200:235–238. http://dx.doi.org/10.1016/0003-2697(92)90458-J

Herz, J., and H.H. Bock. 2002. Lipoprotein receptors in the nervous system. *Annu. Rev. Biochem.* 71:405–434. http://dx.doi.org/10.1146/annurev.biochem.71.110601.135342

Huang, J.C., T. Sakata, L.L. Pfleger, M. Bencsik, B.P. Halloran, D.D. Bikle, and R.A. Nissenson. 2004. PTH differentially regulates expression of RANKL and OPG. *J. Bone Miner. Res.* 19:235–244. http://dx.doi.org/10.1359/JBMR.0301226

Huang, P., Y. Zou, X.Z. Zhong, Q. Cao, K. Zhao, M.X. Zhu, R. Murrell-Lagnado, and X.P. Dong. 2014. P2X4 forms functional ATP-activated cation channels on lysosomal membranes regulated by luminal pH. *J. Biol. Chem.* 289:17658–17667. http://dx.doi.org/10.1074/jbc.M114.552158

Ichihara, A. 2012. (Pro)renin receptor and vacuolar H^+-ATPase. *Keio J. Med.* 61:73–78. http://dx.doi.org/10.2302/kjm.61.73

Idzko, M., D. Ferrari, and H.K. Eltzschig. 2014. Nucleotide signalling during inflammation. *Nature.* 509:310–317. http://dx.doi.org/10.1038/nature13085

Itoh, K., N. Udagawa, K. Matsuzaki, M. Takami, H. Amano, T. Shinki, Y. Ueno, N. Takahashi, and T. Suda. 2000. Importance of membrane- or matrix-associated forms of M-CSF and RANKL/ODF in osteoclastogenesis supported by SaOS-4/3 cells expressing recombinant PTH/PTHrP receptors. *J. Bone Miner. Res.* 15:1766–1775. http://dx.doi.org/10.1359/jbmr.2000.15.9.1766

Khan, T.N., J. Klar, Z. Ali, F. Khan, S.M. Baig, and N. Dahl. 2013. Cenani-Lenz syndrome restricted to limb and kidney anomalies associated with a novel LRP4 missense mutation. *Eur. J. Med. Genet.* 56:371–374. http://dx.doi.org/10.1016/j.ejmg.2013.04.007

Kim, N., A.L. Stiegler, T.O. Cameron, P.T. Hallock, A.M. Gomez, J.H. Huang, S.R. Hubbard, M.L. Dustin, and S.J. Burden. 2008. Lrp4 is a receptor for Agrin and forms a complex with MuSK. *Cell.* 135:334–342. http://dx.doi.org/10.1016/j.cell.2008.10.002

King, B.F. 2007. Novel P2X7 receptor antagonists ease the pain. *Br. J. Pharmacol.* 151:565–567. http://dx.doi.org/10.1038/sj.bjp.0707266

Leupin, O., E. Piters, C. Halleux, S. Hu, I. Kramer, F. Morvan, T. Bouwmeester, M. Schirle, M. Bueno-Lozano, F.J. Fuentes, et al. 2011. Bone overgrowth-associated mutations in the LRP4 gene impair sclerostin facilitator function. *J. Biol. Chem.* 286:19489–19500. http://dx.doi.org/10.1074/jbc.M110.190330

Li, X., Y. Zhang, H. Kang, W. Liu, P. Liu, J. Zhang, S.E. Harris, and D. Wu. 2005. Sclerostin binds to LRP5/6 and antagonizes canonical Wnt signaling. *J. Biol. Chem.* 280:19883–19887. http://dx.doi.org/10.1074/jbc.M413274200

Loots, G.G., M. Kneissel, H. Keller, M. Baptist, J. Chang, N.M. Collette, D. Ovcharenko, I. Plajzer-Frick, and E.M. Rubin. 2005. Genomic deletion of a long-range bone enhancer misregulates sclerostin in Van Buchem disease. *Genome Res.* 15:928–935. http://dx.doi.org/10.1101/gr.3437105

Ma, Y.L., R.L. Cain, D.L. Halladay, X. Yang, Q. Zeng, R.R. Miles, S. Chandrasekhar, T.J. Martin, and J.E. Onyia. 2001. Catabolic effects of continuous human PTH (1--38) in vivo is associated with sustained stimulation of RANKL and inhibition of osteoprotegerin and gene-associated bone formation. *Endocrinology.* 142:4047–4054.

Mahamed, D.A., L.E. Toussaint, and M.S. Bynoe. 2015. CD73-generated adenosine is critical for immune regulation during *Toxoplasma gondii* infection. *Infect. Immun.* 83:721–729. http://dx.doi.org/10.1128/IAI.02536-14

Mediero, A., and B.N. Cronstein. 2013. Adenosine and bone metabolism. *Trends Endocrinol. Metab.* 24:290–300. http://dx.doi.org/10.1016/j.tem.2013.02.001

Mediero, A., F.M. Kara, T. Wilder, and B.N. Cronstein. 2012. Adenosine A(2A) receptor ligation inhibits osteoclast formation. *Am. J. Pathol.* 180:775–786. http://dx.doi.org/10.1016/j.ajpath.2011.10.017

Mediero, A., M. Perez-Aso, and B.N. Cronstein. 2013. Activation of adenosine A(2A) receptor reduces osteoclast formation via PKA- and ERK1/2-mediated suppression of NFκB nuclear translocation. *Br. J. Pharmacol.* 169:1372–1388. http://dx.doi.org/10.1111/bph.12227

Nakashima, T., M. Hayashi, T. Fukunaga, K. Kurata, M. Oh-Hora, J.Q. Feng, L.F. Bonewald, T. Kodama, A. Wutz, E.F. Wagner, et al. 2011. Evidence for osteocyte regulation of bone homeostasis through RANKL expression. *Nat. Med.* 17:1231–1234. http://dx.doi.org/10.1038/nm.2452

Nakayama, M., D. Nakajima, T. Nagase, N. Nomura, N. Seki, and O. Ohara. 1998. Identification of high-molecular-weight proteins with multiple EGF-like motifs by motif-trap screening. *Genomics.* 51:27–34. http://dx.doi.org/10.1006/geno.1998.5341

Narisawa, S., M.C. Yadav, and J.L. Millán. 2013. In vivo overexpression of tissue-nonspecific alkaline phosphatase increases skeletal mineralization and affects the phosphorylation status of osteopontin. *J. Bone Miner. Res.* 28:1587–1598. http://dx.doi.org/10.1002/jbmr.1901

Nguyen, G. 2011. Renin, (pro)renin and receptor: An update. *Clin. Sci.* 120:169–178. http://dx.doi.org/10.1042/CS20100432

Nishikawa, M., T. Akatsu, Y. Katayama, Y. Yasutomo, S. Kado, N. Kugal, M. Yamamoto, and N. Nagata. 1996. Bisphosphonates act on osteoblastic cells and inhibit osteoclast formation in mouse marrow cultures. *Bone.* 18:9–14. http://dx.doi.org/10.1016/8756-3282(95)00426-2

Orimo, H. 2010. The mechanism of mineralization and the role of alkaline phosphatase in health and disease. *J. Nippon Med. Sch.* 77:4–12. http://dx.doi.org/10.1272/jnms.77.4

Orriss, I.R., G.E. Knight, J.C. Utting, S.E. Taylor, G. Burnstock, and T.R. Arnett. 2009. Hypoxia stimulates vesicular ATP release from rat osteoblasts. *J. Cell. Physiol.* 220:155–162. http://dx.doi.org/10.1002/jcp.21745

Orriss, I.R., M.L. Key, M.O. Hajjawi, and T.R. Arnett. 2013. Extracellular ATP released by osteoblasts is a key local inhibitor of bone mineralisation. *PLoS One.* 8:e69057. http://dx.doi.org/10.1371/journal.pone.0069057

Prosdocimo, D.A., D.C. Douglas, A.M. Romani, W.C. O'Neill, and G.R. Dubyak. 2009. Autocrine ATP release coupled to extracellular pyrophosphate accumulation in vascular smooth muscle cells. *Am. J. Physiol. Cell Physiol.* 296:C828–C839. http://dx.doi.org/10.1152/ajpcell.00619.2008

Robinson, D.G., S. Albrecht, and Y. Moriysu. 2004. The V-ATPase inhibitors concanamycin A and bafilomycin A lead to Golgi swelling in tobacco BY-2 cells. *Protoplasma.* 224:255–260. http://dx.doi.org/10.1007/s00709-004-0070-6

Rousselle, A., G. Sihn, M. Rotteveel, and M. Bader. 2014. (Pro)renin receptor and V-ATPase: from *Drosophila* to humans. *Clin. Sci.* 126:529–536. http://dx.doi.org/10.1042/CS20130307

Rudnick, G. 2008. Vesicular ATP transport is a hard (V)NUT to crack. *Proc. Natl. Acad. Sci. USA.* 105:5949–5950. http://dx.doi.org/10.1073/pnas.0802774105

Russell, R.G.G. 2011. Bisphosphonates: The first 40 years. *Bone.* 49:2–19. http://dx.doi.org/10.1016/j.bone.2011.04.022

Ryan, Z.C., T.A. Craig, M. McGee-Lawrence, J.J. Westendorf, and R. Kumar. 2015. Alterations in vitamin D metabolite, parathyroid hormone and fibroblast growth factor-23 concentrations in sclerostin-deficient mice permit the maintenance of a high bone mass. *J. Steroid Biochem. Mol. Biol.* 148:225–231. http://dx.doi.org/10.1016/j.jsbmb.2014.11.021

Sauer, A.V., I. Brigida, N. Carriglio, R.J. Hernandez, S. Scaramuzza, D. Clavenna, F. Sanvito, P.L. Poliani, N. Gagliani, F. Carlucci, et al. 2012. Alterations in the adenosine metabolism and CD39/CD73 adenosinergic machinery cause loss of Treg cell function and autoimmunity in ADA-deficient SCID. *Blood.* 119:1428–1439. http://dx.doi.org/10.1182/blood-2011-07-366781

Semënov, M., K. Tamai, and X. He. 2005. SOST is a ligand for LRP5/LRP6 and a Wnt signaling inhibitor. *J. Biol. Chem.* 280:26770–26775. http://dx.doi.org/10.1074/jbc.M504308200

Shen, C., W.C. Xiong, and L. Mei. 2014. Caspase-3, shears for synapse pruning. *Dev. Cell.* 28:604–606. http://dx.doi.org/10.1016/j.devcel.2014.03.010

Shen, C., W.C. Xiong, and L. Mei. 2015. LRP4 in neuromuscular junction and bone development and diseases. *Bone.* 80:101–108. http://dx.doi.org/10.1016/j.bone.2015.05.012

Silvestrini, G., P. Ballanti, M. Sebastiani, M. Leopizzi, M. Di Vito, and E. Bonucci. 2008. OPG and RANKL mRNA and protein expressions in the primary and secondary metaphyseal trabecular bone of PTH-treated rats are independent of that of SOST. *J. Mol. Histol.* 39:237–242. http://dx.doi.org/10.1007/s10735-007-9158-6

Suzuki, T. 2004. Identification of novel PSD proteins and their possible functions. [In Japanese.] *Nihon Shinkei Seishin Yakurigaku Zasshi.* 24:205–210.

Takahashi, N., K. Maeda, A. Ishihara, S. Uehara, and Y. Kobayashi. 2011. Regulatory mechanism of osteoclastogenesis by RANKL and Wnt signals. *Front. Biosci. (Landmark Ed.).* 16:21–30. http://dx.doi.org/10.2741/3673

Takai, E., M. Tsukimoto, H. Harada, and S. Kojima. 2014. Autocrine signaling via release of ATP and activation of P2X7 receptor influences motile activity of human lung cancer cells. *Purinergic Signal.* 10:487–497. http://dx.doi.org/10.1007/s11302-014-9411-x

Teitelbaum, S.L. 2000. Bone resorption by osteoclasts. *Science.* 289:1504–1508. http://dx.doi.org/10.1126/science.289.5484.1504

Tian, Q.B., K. Nakayama, A. Okano, and T. Suzuki. 1999. Identification of mRNAs localizing in the postsynaptic region. *Brain Res. Mol. Brain Res.* 72:147–157. http://dx.doi.org/10.1016/S0169-328X(99)00214-4

Tokunaga, A., M. Tsukimoto, H. Harada, Y. Moriyama, and S. Kojima. 2010. Involvement of SLC17A9-dependent vesicular exocytosis in the mechanism of ATP release during T cell activation. *J. Biol. Chem.* 285:17406–17416. http://dx.doi.org/10.1074/jbc.M110.112417

Trepiccione, F., S.D. Gerber, F. Grahammer, K.I. López-Cayuqueo, V. Baudrie, T.G. Păunescu, D.E. Capen, N. Picard, R.T. Alexander, T.B. Huber, et al. 2016. Renal Atp6ap2/(pro)renin receptor is required for normal vacuolar H+-ATPase function but not for the renin-angiotensin system. *J. Am. Soc. Nephrol.* 27:3320–3330. http://dx.doi.org/10.1681/ASN.2015080915

Wang, D., and P.R. Hiesinger. 2013. The vesicular ATPase: A missing link between acidification and exocytosis. *J. Cell Biol.* 203:171–173. http://dx.doi.org/10.1083/jcb.201309130

Weatherbee, S.D., K.V. Anderson, and L.A. Niswander. 2006. LDL-receptor-related protein 4 is crucial for formation of the neuromuscular junction. *Development.* 133:4993–5000. http://dx.doi.org/10.1242/dev.02696

Wijenayaka, A.R., M. Kogawa, H.P. Lim, L.F. Bonewald, D.M. Findlay, and G.J. Atkins. 2011. Sclerostin stimulates osteocyte support of osteoclast activity by a RANKL-dependent pathway. *PLoS One.* 6:e25900. http://dx.doi.org/10.1371/journal.pone.0025900

Wu, H., W.C. Xiong, and L. Mei. 2010. To build a synapse: Signaling pathways in neuromuscular junction assembly. *Development.* 137:1017–1033. http://dx.doi.org/10.1242/dev.038711

Wu, H., Y. Lu, C. Shen, N. Patel, L. Gan, W.C. Xiong, and L. Mei. 2012. Distinct roles of muscle and motoneuron LRP4 in neuromuscular junction formation. *Neuron.* 75:94–107. http://dx.doi.org/10.1016/j.neuron.2012.04.033

Xia, W.F., F.L. Tang, L. Xiong, S. Xiong, J.U. Jung, D.H. Lee, X.S. Li, X. Feng, L. Mei, and W.C. Xiong. 2013. Vps35 loss promotes hyperresorptive osteoclastogenesis and osteoporosis via sustained RANKL signaling. *J. Cell Biol.* 200:821–837. http://dx.doi.org/10.1083/jcb.201207154

Xiong, J., M. Onal, R.L. Jilka, R.S. Weinstein, S.C. Manolagas, and C.A. O'Brien. 2011. Matrix-embedded cells control osteoclast formation. *Nat. Med.* 17:1235–1241. http://dx.doi.org/10.1038/nm.2448

Xiong, L., J.U. Jung, H. Wu, W.F. Xia, J.X. Pan, C. Shen, L. Mei, and W.C. Xiong. 2015. Lrp4 in osteoblasts suppresses bone formation and promotes osteoclastogenesis and bone resorption. *Proc. Natl. Acad. Sci. USA.* 112:3487–3492. http://dx.doi.org/10.1073/pnas.1419714112

Yasuda, H., N. Shima, N. Nakagawa, K. Yamaguchi, M. Kinosaki, S. Mochizuki, A. Tomoyasu, K. Yano, M. Goto, A. Murakami, et al. 1998. Osteoclast differentiation factor is a ligand for osteoprotegerin/osteoclastogenesis-inhibitory factor and is identical to TRANCE/RANKL. *Proc. Natl. Acad. Sci. USA.* 95:3597–3602. http://dx.doi.org/10.1073/pnas.95.7.3597

Zaiss, M.M., M. Kurowska-Stolarska, C. Böhm, R. Gary, C. Scholtysek, B. Stolarski, J. Reilly, S. Kerr, N.L. Millar, T. Kamradt, et al. 2011. IL-33 shifts the balance from osteoclast to alternatively activated macrophage differentiation and protects from TNF-alpha-mediated bone loss. *J. Immunol.* 186:6097–6105. http://dx.doi.org/10.4049/jimmunol.1003487

Zhang, B., S. Luo, Q. Wang, T. Suzuki, W.C. Xiong, and L. Mei. 2008. LRP4 serves as a coreceptor of agrin. *Neuron.* 60:285–297. http://dx.doi.org/10.1016/j.neuron.2008.10.006

Zhang, J., Y. Feng, and M. Forgac. 1994. Proton conduction and bafilomycin binding by the V0 domain of the coated vesicle V-ATPase. *J. Biol. Chem.* 269:23518–23523.

Zhang, M., S. Xuan, M.L. Bouxsein, D. von Stechow, N. Akeno, M.C. Faugere, H. Malluche, G. Zhao, C.J. Rosen, A. Efstratiadis, and T.L. Clemens. 2002. Osteoblast-specific knockout of the insulin-like growth factor (IGF) receptor gene reveals an essential role of IGF signaling in bone matrix mineralization. *J. Biol. Chem.* 277:44005–44012. http://dx.doi.org/10.1074/jbc.M208265200

Zhao, C., N. Irie, Y. Takada, K. Shimoda, T. Miyamoto, T. Nishiwaki, T. Suda, and K. Matsuo. 2006. Bidirectional ephrinB2-EphB4 signaling controls bone homeostasis. *Cell Metab.* 4:111–121. http://dx.doi.org/10.1016/j.cmet.2006.05.012

Zong, Y., B. Zhang, S. Gu, K. Lee, J. Zhou, G. Yao, D. Figueiredo, K. Perry, L. Mei, and R. Jin. 2012. Structural basis of agrin-LRP4-MuSK signaling. *Genes Dev.* 26:247–258. http://dx.doi.org/10.1101/gad.180885.111